Development of an inertial confinement fusion platform to study charged-particle-producing nuclear reactions relevant to nuclear astrophysics

M. Gatu Johnson, A. B. Zylstra, A. Bacher, C. R. Brune, D. T. Casey, C. Forrest, H. W. Herrmann, M. Hohenberger, D. B. Sayre, R. M. Bionta, J.-L. Bourgade, J. A. Caggiano, C. Cerjan, R. S. Craxton, D. Dearborn, M. Farrell, J. A. Frenje, E. M. Garcia, V. Yu. Glebov, G. Hale, E. P. Hartouni, R. Hatarik, M. Hohensee, D. M. Holunga, M. Hoppe, R. Janezic, S. F. Khan, J. D. Kilkenny, Y. H. Kim, J. P. Knauer, T. R. Kohut, B. Lahmann, O. Landoas, C. K. Li, F. J. Marshall, L. Masse, A. McEvoy, P. McKenty, D. P. McNabb, A. Nikroo, T. G. Parham, M. Paris, R. D. Petrasso, J. Pino, P. B. Radha, B. Remington, H. G. Rinderknecht, H. Robey, M. J. Rosenberg, B. Rosse, M. Rubery, T. C. Sangster, J. Sanchez, M. Schmitt, M. Schoff, F. H. Séguin, W. Seka, H. Sio, C. Stoeckl, and R. E. Tipton

Citation: Physics of Plasmas **24**, 041407 (2017); doi: 10.1063/1.4979186

View online: http://dx.doi.org/10.1063/1.4979186

View Table of Contents: http://aip.scitation.org/toc/php/24/4

Published by the American Institute of Physics

Development of an inertial confinement fusion platform to study charged-particle-producing nuclear reactions relevant to nuclear astrophysics

M. Gatu Johnson,[1] A. B. Zylstra,[2] A. Bacher,[3] C. R. Brune,[4] D. T. Casey,[5] C. Forrest,[6] H. W. Herrmann,[2] M. Hohenberger,[6] D. B. Sayre,[5] R. M. Bionta,[5] J.-L. Bourgade,[7] J. A. Caggiano,[5] C. Cerjan,[5] R. S. Craxton,[6] D. Dearborn,[5] M. Farrell,[8] J. A. Frenje,[1] E. M. Garcia,[6] V. Yu. Glebov,[6] G. Hale,[2] E. P. Hartouni,[5] R. Hatarik,[5] M. Hohensee,[5] D. M. Holunga,[5] M. Hoppe,[8] R. Janezic,[6] S. F. Khan,[5] J. D. Kilkenny,[8] Y. H. Kim,[2] J. P. Knauer,[6] T. R. Kohut,[5] B. Lahmann,[1] O. Landoas,[7] C. K. Li,[1] F. J. Marshall,[6] L. Masse,[5] A. McEvoy,[2] P. McKenty,[6] D. P. McNabb,[5] A. Nikroo,[5] T. G. Parham,[5] M. Paris,[2] R. D. Petrasso,[1] J. Pino,[5] P. B. Radha,[6] B. Remington,[5] H. G. Rinderknecht,[5] H. Robey,[5] M. J. Rosenberg,[6] B. Rosse,[7] M. Rubery,[9] T. C. Sangster,[6] J. Sanchez,[5] M. Schmitt,[2] M. Schoff,[8] F. H. Séguin,[1] W. Seka,[6] H. Sio,[1] C. Stoeckl,[6] and R. E. Tipton[5]

[1]*Massachusetts Institute of Technology, Cambridge, Massachusetts 02139, USA*
[2]*Los Alamos National Laboratory, Los Alamos, New Mexico 87544, USA*
[3]*Indiana University, Bloomington, Indiana 47405, USA*
[4]*Ohio University, Athens, Ohio 45701, USA*
[5]*Lawrence Livermore National Laboratory, Livermore, California 94550, USA*
[6]*Laboratory for Laser Energetics, University of Rochester, Rochester, New York 14623, USA*
[7]*CEA, DAM, DIF, F-91297 Arpajon, France*
[8]*General Atomics, San Diego, California 92186, USA*
[9]*Plasma Physics Department, AWE plc, Reading RG7 7PR, United Kingdom*

(Received 14 October 2016; accepted 12 December 2016; published online 28 March 2017)

This paper describes the development of a platform to study astrophysically relevant nuclear reactions using inertial-confinement fusion implosions on the OMEGA and National Ignition Facility laser facilities, with a particular focus on optimizing the implosions to study charged-particle-producing reactions. Primary requirements on the platform are high yield, for high statistics in the fusion product measurements, combined with low areal density, to allow the charged fusion products to escape. This is optimally achieved with direct-drive exploding pusher implosions using thin-glass-shell capsules. Mitigation strategies to eliminate a possible target sheath potential which would accelerate the emitted ions are discussed. The potential impact of kinetic effects on the implosions is also considered. The platform is initially employed to study the complementary T(t,2n)α, T(^{3}He,np)α and ^{3}He(^{3}He,2p)α reactions. Proof-of-principle results from the first experiments demonstrating the ability to accurately measure the energy and yields of charged particles are presented. Lessons learned from these experiments will be used in studies of other reactions. The goals are to explore thermonuclear reaction rates and fundamental nuclear physics in stellar-like plasma environments, and to push this new frontier of nuclear astrophysics into unique regimes not reachable through existing platforms, with thermal ion velocity distributions, plasma screening, and low reactant energies. *Published by AIP Publishing*. [http://dx.doi.org/10.1063/1.4979186]

I. INTRODUCTION

Thermonuclear reactions relevant to stellar nucleosynthesis (SN) and big-bang nucleosynthesis (BBN) have been explored traditionally by means of accelerator experiments.[1] High-energy-density (HED) plasmas generated in inertial confinement fusion (ICF) experiments at large lasers such as OMEGA[2] and the National Ignition Facility (NIF)[3,4] more closely mimic an astrophysical environment in several ways. The target nuclei in accelerator experiments are surrounded by bound electrons, while electrons occupy mainly continuum states in stars and in HED plasmas. Unsatisfactory systematic uncertainties are introduced by the two-step theoretical corrections currently required to go from laboratory-measured reaction rates with bound electron screening via projected bare nucleus rates to stellar rates with plasma screening.[1,5,6] Accelerator experiments also use a mono-energetic ion beam to initiate reactions, while reactions in stars and HED plasmas occur within populations of ions with thermal velocity distributions. Additionally, due to the very low reaction rates at energies relevant to SN, accurate accelerator measurements also require very long beam times (of order months) and extremely low background environments, such as can only be achieved in underground facilities like the Laboratory for Underground Nuclear Astrophysics (LUNA).[7] These challenges further motivate work to develop a new method for probing these reactions.

Astrophysical conditions span a broad range of temperatures and densities. During BBN, nuclei were formed in the time window 200–1000 s, when temperatures were in the range of 30–80 keV (86 keV–10^9 K).[1] The energy-producing fusion reactions in our sun, which is currently in the main sequence, occur at a temperature of ∼1.3 keV. Higher-mass stars and later stages of stellar burning (e.g., core helium burn, shell burn) occur at higher temperatures (Fig. 1(a)). Conditions similar to those in stars can be closely replicated[8]

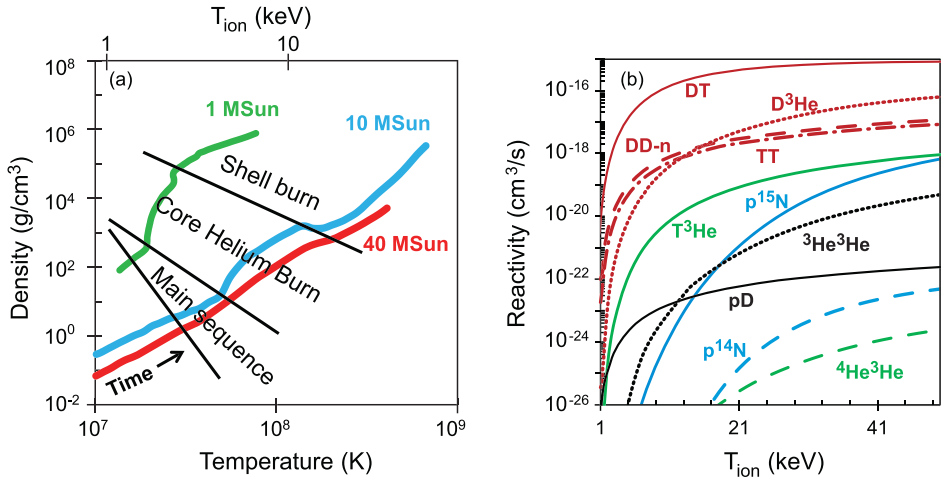

FIG. 1. (a) Typical density and temperature conditions under which fusion reactions occur in stars with mass equivalent to 1 solar mass (1 MSun, green), 10 MSun (blue), and 40 MSun (red) evolve over time (from left to right in the figure) as the star passes through the main sequence, core helium burn and shell burn. Note that while time moves from left to right in the figure, the absolute time scale is different for each trace—lighter stars evolve much slower than heavier stars. (b) Reactivities for SN and BBN-relevant reactions are generally low and decrease rapidly with decreasing temperature. Here, as an example, BBN-relevant reactions $T(^3He,d)\alpha$ and $^3He(\alpha,\gamma)^7Be$ are shown in green, proton-proton-chain-relevant reactions $D(p,\gamma)^3He$ and $^3He(^3He,2p)\alpha$ in black, CNO-relevant reactions $^{15}N(p,\alpha)^{12}C$ and $^{14}N(p,\gamma)^{15}O$ in blue, and reference reactions $D(T,n)\alpha$, $D(D,n)^3He$, $D(^3He,p)\alpha$, and $T(T,2n)\alpha$ in red.

in HED plasma physics experiments, where ion temperatures (T_{ion}) up to ~30 keV (Ref. 9) and areal densities (ρR) up to ~1.3 g/cm^2 (Ref. 10; corresponding to densities ranging from many tens of g/cm^3 in the center of the implosion to many hundreds of g/cm^3 in the surrounding dense fuel layer) have been demonstrated.

The use of HED plasmas to study nuclear reactions relevant to SN and BBN has recently begun with implosion experiments at the OMEGA laser[11,12] and a first series of experiments currently underway at the NIF. This work builds on the successful use of plasmas[13] and the HED platform[14–16] to probe fundamental nuclear physics problems. The feasibility of accurate reaction-rate measurements using HED plasmas by exploiting the yield ratio between the reaction of interest and a well-known reference reaction has also been recently confirmed.[8] In this paper, considerations for optimizing the HED platform for measurements of charged-particle producing SN and BBN-relevant reactions are discussed, and results from the first platform development experiments at both OMEGA and the NIF are presented. The ultimate goals of these efforts are to explore thermonuclear reaction rates and relevant fundamental nuclear physics in stellar-like plasma environments, compare results to traditional accelerator experiments, and push the frontier into regimes not reachable through existing platforms (with thermal ion velocity distributions, plasma screening, and low reactant energies).

Reactivities for nucleosynthesis-relevant reactions[17] are generally low, and increase very strongly with T_{ion} (Fig. 1(b)). Given the low reactivities, the primary requirement on a platform designed to study astrophysically relevant nuclear reactions is high yield. Generally, the higher the yield from an implosion, the more straightforward it will be to obtain sufficient statistics in fusion product measurements. For charged-particle-producing reactions, an additional necessary platform requirement is minimal spectral distortions. Escaped charged-particle spectra can be distorted either through energy upshifts due to capsule charging, or through energy loss in the assembled plasma.[18] Energy loss scales directly with implosion ρR, which must thus be minimized for these implosions. Charging of ICF capsules has been found to occur because of hot electrons generated by the two-plasmon decay (TPD) instability.[19,20] Hot-electron production due to the TPD instability scales with laser intensity above a threshold ~2–5 × 10^{14} W/cm^2 depending on plasma conditions.[20] The associated positive target potential, responsible for upshifts of fusion products, decays fairly rapidly after laser turn-off.[18,19] In practice, this means that there are two paths to minimizing charged-particle spectral distortion due to capsule charging, (i) to keep the laser intensity below the threshold for TPD onset, or (ii) to design the implosion so that peak nuclear production (bang time (BT)) occurs after the end of the laser pulse. Here, we have chosen the second option, because reducing the laser intensity below the TPD threshold also reduces achievable implosion yields and makes it more challenging to achieve low ρR. For many of the reactions relevant to SN, optimizing the implosions for low (by HED standards) T_{ion} also increases the relevance for stellar scenarios. In these cases, the platform design comes down to a balance game of generating sufficient yield at lowest possible T_{ion}. In this paper, efforts to develop optimized experimental designs considering these criteria to probe charged-particle-producing reactions relevant to SN on OMEGA and the NIF are described.

The structure of the paper is as follows: Sec. II details design considerations for OMEGA experiments; Sec. III results from initial OMEGA experiments. Section IV discusses design considerations for NIF experiments, and Sec. V results from initial NIF measurements. In Sec. VI, some aspects of data interpretation common to NIF and OMEGA are discussed; in particular, how does the fact that these ICF implosions are not uniform in density and temperature over the burn duration and region impact how we interpret the data? Finally, future directions and planned platform improvements are discussed in Sec. VII, and Section VIII concludes the paper.

II. OMEGA EXPERIMENT DESIGN

The dual platform requirements of high yield and minimal ρR are optimally met with shock-driven, thin-glass-shell capsule "exploding pusher" implosions. Design optimization for the first round of platform development experiments on OMEGA focused on selecting the optimal target parameters—outer diameter (OD), shell thickness, and fill pressure (P)—to maximize yield and minimize ρR at maximum laser power. Optimal laser pulse duration was also considered. These first implosions were designed to measure the neutron and alpha fusion product spectra from the tritium-tritium T(t,2n)α reaction, a mirror reaction to ^{3}He(^{3}He,2p)α, which is responsible for nearly half the energy production in our sun.[1]

1D ARES[21]-simulated TT neutron (TT-n) yield, burn-averaged T_{ion} and ρR for two T_2 fill pressures (P = 5 atm and P = 10 atm), and three ODs (OD = 860 μm, 920 μm, and 1160 μm) are shown versus shell thickness in Fig. 2. These simulations were all run with a 1 ns square laser pulse with realistic wiggles and laser energy $E_{laser} \sim 28$ kJ. 75% of the laser energy was assumed to be absorbed by the capsule, and a flux limiter of 0.07 was used. Reactions from zones with $T_{ion} > 25$ keV were excluded in the post-processing to minimize spurious values from central zones, where a numerical singularity in 1D creates unphysical temperatures. The model also included 0.25 atm residual CO_2. The first important observation is that ρR varies relatively slowly, and is acceptably low, for shell thickness $\lesssim 3$ μm. Yield is seen to climb over the range of shell thicknesses plotted for all but the largest capsules (OD = 1160 μm), which show a pressure-dependent roll-over (the yield starts to fall earlier with shell thickness for the 10 atm fill case than for the 5 atm fill).

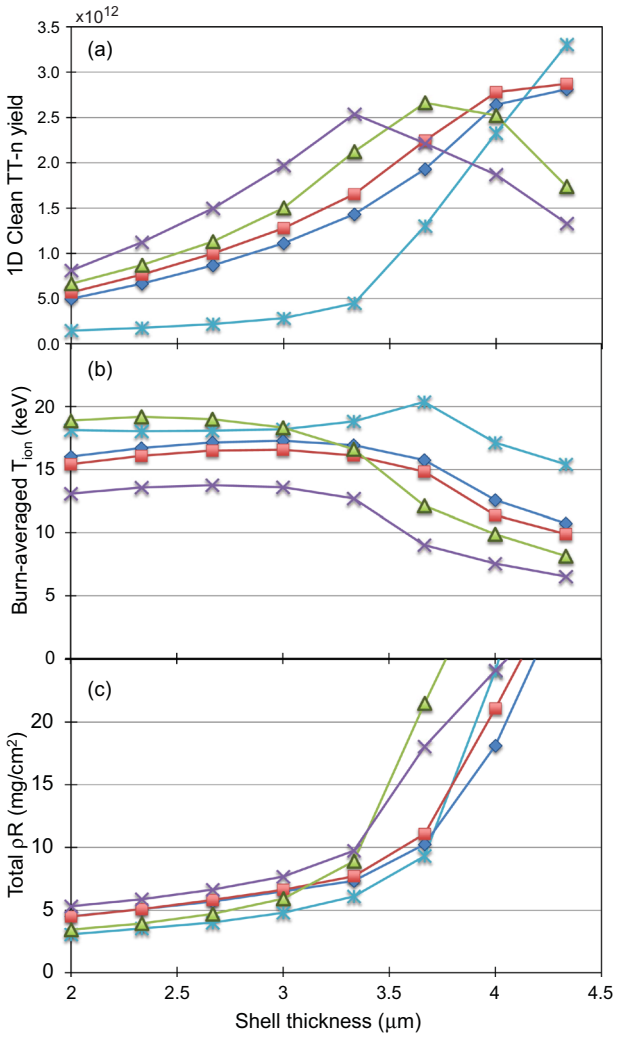

FIG. 2. (a) TT-n yield, (b) burn-averaged T_{ion}, and (c) total ρR from 1D ARES simulations of OMEGA-scale implosions versus SiO_2-capsule shell thickness (see text for details). Blue stars represent capsules with 5 atm T_2 fill and 860 μm OD, blue diamonds capsules with 10 atm T_2 fill and 860 μm OD, red squares capsules with 10 atm T_2 fill and 920 μm OD, green triangles capsules with 5 atm T_2 fill and 1160 μm OD, and purple crosses capsules with 10 atm T_2 fill and 1160 μm OD. Note in particular how simulated total ρR (bottom panel) starts to climb rapidly for shell thickness > 3 μm.

Based on these simulations, 1000 μm OD capsules with 3.0 μm-thick shells and ~10 atm T_2 fill were selected for the first round of T_2 implosions to maximize yield at an acceptable (~5 mg/cm^2) ρR. The database of past DT-gas-filled thin-glass-shell OMEGA implosions (2004–2010) was also studied to confirm the fidelity of the simulation results (Fig. 3). Not only shell thickness but also capsule diameter, fill pressure, and laser energy vary between different implosions, which has to be considered when studying Fig. 3. The available data suggest that a DT yield of $\sim 6 \times 10^{13}$ is obtained around a shell thickness of 3.0 μm and OD = 1000 μm for a fill pressure of ~10 atm for these 50:50 D:T implosions, which scales to a TT-n yield of $\sim 10^{12}$, roughly consistent with the simulated result.

Simulations and past data also show that if a 1000 μm OD capsule with a 3.0 μm-thick shell and ~10 atm fill is shot with a 1 ns square, full power laser pulse, bang time (BT) will occur during the laser pulse. As discussed above, this can be expected to lead to charged-particle energy upshift due to capsule charging.[18] This motivated running a simulation with a 0.6 ns laser pulse at full power for comparison. The ARES simulations predict a minimal TT-n yield reduction of 4.9% by going from the 1.0 ns to the 0.6 ns pulse. DT bang times of 864 ps for the 0.6 ns case and 896 ps for the 1.0 ns case are predicted, which indicates that at a minimal cost in yield, the outlook for undistorted charged-particle measurements is much improved.

So far, we have not discussed T_{ion} at all. As can be seen in Fig. 2, T_{ion} is predicted to stay fairly constant as a function of shell thickness for the nominal drive conditions for thicknesses $\lesssim 3.0$ μm, and to drop towards higher shell thicknesses (although this would come at the expense of higher ρR). Predicted T_{ion} for these implosions is generally fairly high; optimizing for low T_{ion} was not a primary goal for the first OMEGA experiments. It is interesting to note, however, that if we relax the ρR requirements, T_{ion} can be significantly varied using the same glass capsules by changing the fill pressure/laser pulse combination. This was tested in the first round of platform development experiments at OMEGA (see Section III below).

III. OMEGA EXPERIMENT RESULTS

Table I summarizes implosion parameters and results for the first platform development T(t, 2n)α experiments on OMEGA November 2012-January 2013 (shots 67 941–68 448). These implosions all used SG4 phase plates, but smoothing by spectral dispersion (SSD) was not applied.

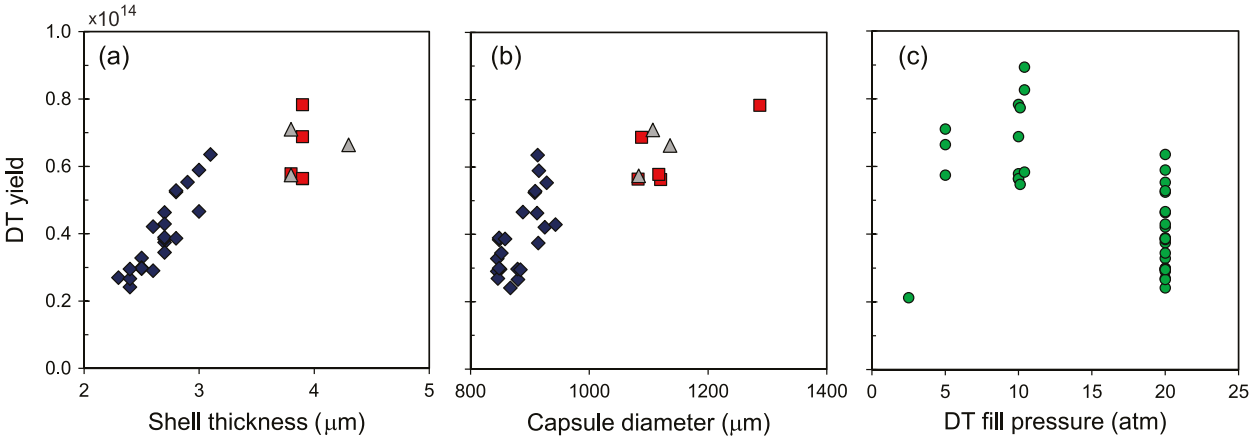

FIG. 3. Data from OMEGA DT exploding pusher implosions from 2004 to 2010 showing DT yield dependence on (a) SiO_2 shell thickness, (b) capsule diameter, and (c) DT fill pressure. Blue diamonds represent implosions with 20 atm DT fill shot with 28–30 kJ laser energy on target, red squares implosions with 10 atm DT fill shot with 20–25 kJ laser energy, gray triangles capsules with 5 atm DT fill shot with 25–28 kJ laser energy, and green circles implosions with 2.4–4.4 μm thick SiO_2 shells shot with 20–30 kJ laser energy. The spread in the plotted data is expected as shell thickness, capsule diameter, fill pressure, and laser energy each individually impact yield performance and more than one such implosion parameter varies within each set of data points.

For comparison, results from similar experiments in July 2015 (shots 77 951–77 964) are also shown. Two reconfigurations of the OMEGA facility happened between the two series of shots—new, smaller SG5 phase plates were introduced, and an arbitrary waveform generator (AWG) was implemented (this is why the pulse shapes change names between the two sets of shots; nominally, SG0604 = SG06v001 and RM2002 = RM20v001). The TT-n yields were measured with a highly collimated, well-shielded neutron time-of-flight (nTOF) detector at 13.4 m from the target chamber center (TCC) with the capability of gating out the faster neutrons from the DT reaction;[22] for shots 67 952–67 963, a bibenzyl scintillation crystal was used, while shots 67 941, 68 448, and 77 951–77 964 used an oxygenated xylene scintillator. (On shots 67 952–67 963, independent TT-n yield measurements were also made with the magnetic recoil spectrometer (MRS) neutron spectrometer and with indium, aluminum, and copper activation; good agreement was found between the three methods, see Appendix A.) DT T_{ion} for shots 67 941–68 448 was measured with the 12mntofh detector,[23] DT T_{ion} for 77 951–77 964 with the 13.4 m LaCave nTOF detector. Bang times were measured with the neutron temporal diagnostic (NTD)[24] (the uncertainty in the measured DT BT is $\sim\pm$50 ps).

The first thing to note when studying Table I is that the performance for nominally identical implosions is remarkably stable over time, in spite of the facility changes

TABLE I. Parameters of 13 tritium-gas filled, glass-shell implosions run in the first series of OMEGA experiments using the platform described in this paper (November 2012-January 2013; shots 67 941-68 448), and of an additional 5 comparable implosions from July 2015 (shots 77 951-77 964). Laser pulse shapes SG0604 and SG06v001 are nominally the same, 0.6 ns square, SG1018 is 1.0 ns square, and RM2002 and RM20v001 are nominally the same, 2 ns ramped (see Fig. 4).

Shot	Pulse shape	Laser energy (kJ)	Lens position (mm)	Capsule diameter (μm)	Shell thickness (μm)	T_2 fill pressure (atm)	TT-n yield ($\times 10^{12}$)	DT T_{ion} (keV)	DT bang time (ps)
67 952	SG0604	17.5	0	1006	2.9	10.0 ± 0.2	1.40 ± 0.16	13.2 ± 0.5	843
67 953	SG0604	17.7	0	1007	2.9	10.0 ± 0.2	1.40 ± 0.16	12.8 ± 0.5	867
67 954	SG0604	17.8	0	1008	2.9	10.0 ± 0.2	1.16 ± 0.14	13.8 ± 0.5	888
67 955	SG1018	29.7	0	1012	2.9	9.9 ± 0.2	1.24 ± 0.14	13.8 ± 0.5	878
67 956	SG1018	29.2	0	1012	2.9	10.0 ± 0.2	1.35 ± 0.16	13.2 ± 0.5	917
67 958	SG1018	28.8	0	1013	2.9	10.0 ± 0.2	1.21 ± 0.14	12.8 ± 0.5	905
67 959	SG1018	29.3	0	1017	3.0	10.0 ± 0.2	1.42 ± 0.17	13.1 ± 0.5	911
67 960	RM2002	22.4	0	1011	3.0	10.0 ± 0.2	0.59 ± 0.07	7.5 ± 0.5	…
67 961	RM2002	22.4	0	1028	3.3	9.9 ± 0.2	0.55 ± 0.06	6.7 ± 0.5	1619
67 962	RM2002	22.8	0	1021	3.3	10.0 ± 0.2	0.55 ± 0.06	6.5 ± 0.5	1594
67 963	RM2002	23.2	0	1011	3.3	9.9 ± 0.2	0.60 ± 0.07	6.6 ± 0.5	1516
67 941	RM2002	23.6	7.3	1027	3.3	9.9 ± 0.2	0.18 ± 0.02	4.1 ± 0.5	…
68 448	RM2002	21.1	7.3	1007	2.9	9.9 ± 0.3	0.13 ± 0.01	4.0 ± 0.5	…
77 951	SG06v001	16.1	0	1004	2.9	3.3	0.49 ± 0.05	18.3 ± 0.5	756
77 952	SG06v001	15.9	0	1005	2.9	3.3	0.40 ± 0.04	17.7 ± 0.5	731[a]
77 960	SG06v001	16.1	0	1004	2.9	8.2	1.27 ± 0.14	11.1 ± 0.5	806[a]
77 963	RM20v001	24.1	7.3	1009	3.0	8.2	0.24 ± 0.03	3.7 ± 0.5	1689[a]
77 964	RM20v001	19.3	7.3	1007	2.9	8.2	0.13 ± 0.01	3.4 ± 0.5	1763[a]

[a]Data from the new cryoNTD detector; all other bang times measured with the old H5 NTD.

mentioned and in spite of the diagnostic changes between implosions (compare shots 67 952–67 954 and shot 77 960, and shots 67 941, 68 448, 77 963, and 77 964). The second thing to note is that the agreement with 1D simulations is remarkably good. The 1D ARES-predicted TT-n yield for the 1-ns square laser pulse implosions is $\sim 1.4 \times 10^{12}$ (Fig. 2(a)), while the measured average for these implosions is 1.3×10^{12} with an uncertainty (dominated by systematics) of ~11%. ARES predicts a 4.9% increase in TT-n yield going from a 0.6 ns to a 1.0 ns square pulse; on average, a 1.1% reduction in TT yield is observed. For comparison, ARES predicts a 3.7% increase in DT yield, while on average, an increase of 14% is observed. (DT yields are not shown in the table because the deuterium impurity (~1.5%) in the T_2 fill is not well known, see Appendix B.) This confirms the conclusion from simulations that only minimal (if any) yield reduction is expected when going from a 1.0 ns to a 0.6 ns square pulse for a capsule of these dimensions. Further, ARES also predicts a DT BT of 864 ps for the 0.6 ns case and a DT BT of 896 ps for the 1.0 ns case; average DT BTs of 866 ps and 891 ps are observed, again in remarkable agreement with the (pre-shot) 1D simulation.

Backscattered laser light was also measured on these experiments.[25] From these measurements, an absorbed laser light fraction of ~66% was observed for the high-intensity 0.6-ns and 1.0-ns square laser pulses, while for the lower intensity RM2002 laser pulse shots, ~75% of the laser light was absorbed by the capsule. When comparing the simulations and measurements, it should be kept in mind that a slightly higher capsule absorption (75%) was assumed in the simulations.

In addition to the 0.6 ns and 1.0 ns square pulse cases, a 2 ns ramped laser pulse was also shot with two different focusing settings (best-focus, with the lens position set to 0 mm, and de-focus, with the lens position set to 7.3 mm; the lens is a component of the final optics for each laser beam that determines the beam focus[26]). In July 2015, a lower fill pressure ($P_{T2} \sim 3.3$ atm) was also shot. The purpose of these variations was to vary T_{ion} to study the energy dependence of the T(t, 2n)α reaction. As can be seen in Table I, T_{ion} ranging from 3.4 keV to 18.3 keV was achieved this way. The highest T_{ion} of 18.3 keV is obtained by driving the capsule with the lower fill pressure with a square pulse, leading to a fast, entirely shock-driven implosion. The lowest T_{ion} of 3.4 keV is obtained by imploding a higher fill-pressure capsule with the lower-intensity 2 ns ramped pulse and defocusing the laser beams, thus driving the implosion slower and more compressively.

Fig. 4 shows the laser pulse shapes and NTD-measured burn histories from shots 67 953, 67 956, and 67 961. The laser pulse shapes are representative for the 0.6 ns square, 1.0 ns square, and 2 ns ramped cases, respectively. Note that the DT neutron burn histories for the 0.6 ns square (black) and 1.0 ns square (red) cases are very similar, with burn happening well within the laser pulse for the 1.0 ns square case and after the end of the laser pulse for the 0.6 ns case. For these two implosion types, the NTD was fielded 20 cm from TCC to avoid saturation because of the relatively high yield. For the 2 ns ramped case (shot 67 961, blue), NTD could be moved to 10 cm from TCC, which reduced the time separation between the DT and TT neutrons. The closer fielding distance also reduces the time spread for the TT neutron spectrum, which extends over energies ~0–9 MeV, making the TT signal stronger relative to DT. In this case, the TT neutrons can also be seen in the trace (from ~2000 to 3000 ps; note that the time window covered by the NTD streak camera sweep time also changes with the fielding distance, which contributes to the TT signal being visible for 67 961 and not for 67 953 and 67 956). Bang time happens well within the laser pulse also for the 2.0 ns ramped case, but we will see below that the charged-particle spectral distortions are still dominated by downshift due to ρR because of the higher convergence obtained when the implosion is driven this way.

The success in optimizing these implosions for minimal distortion in charged particle measurements can be evaluated by studying the alpha particle spectra measured by two charged-particle spectrometers[27] (CPS1 & CPS2). An example alpha spectrum measured by CPS2 for shot 67 952 is shown in Fig. 5. The DT alphas ($E_\alpha \sim 3.6$ MeV) clearly dominate the measurement. The TT-alpha spectrum is expected to cover the range from 0–4 MeV, but cannot be reliably measured in these implosions with ~1.5% deuterium because of the high DT yield. A hint of TT alphas can be seen in the range 1.5–2.0 MeV, but the shape of the TT alpha spectrum cannot be trusted because of possible contamination from scattered DT-alpha and challenges in the subtraction of a background of accelerated Si and O from the capsule shell towards the low end of this energy range. Also shown in the plot is the expected DT alpha spectrum, broadened and upshifted[28] consistent with T_{ion} inferred from DT neutron measurements on this shot (13.2 keV; red curve). The measured spectrum appears slightly downshifted and slightly broadened relative to the expectation (a $T_{ion} = 18.8$ keV is inferred from the DT-α spectrum, neglecting additional broadening due to ρR evolution or the decaying target potential[18]), but given the relatively high stopping power for alpha particles,[29] the agreement for this 0.6 ns pulse shape shot is remarkably good, demonstrating that the goal of designing an implosion where charged-particle spectra escape undistorted was met.

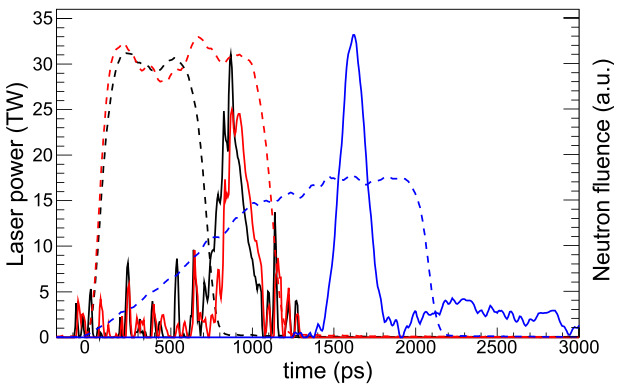

FIG. 4. Laser pulse shapes (dashed lines, left axis) and NTD data (solid lines, right axis, arbitrary units) from three example shots, 67 953 shot with the SG0604 0.6 ns square pulse shape in black, 67 956 shot with the SG1018 1.0 ns square pulse shape in red, and 67 961 shot with the RM2002 2 ns ramped laser pulse in blue, all with best focus (0 mm lens position). Note that burn happens after the end of the laser pulse only for the 0.6 ns pulse case (black).

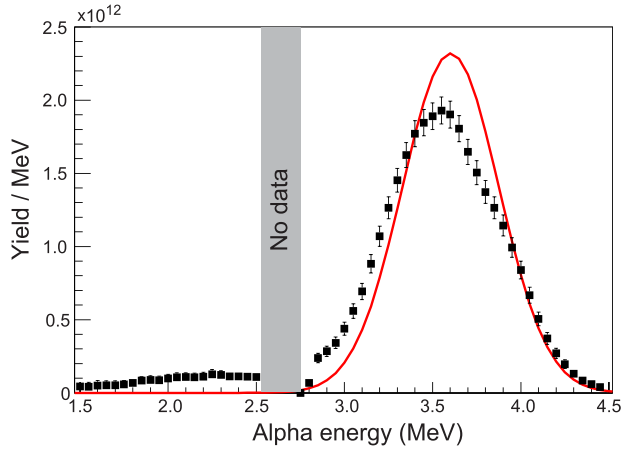

FIG. 5. Example alpha spectrum measured by CPS2 on shot 67 952 (black points with error bars). Also shown is the expected nominal shape for the DT alpha spectrum for this shot (broadened and upshifted consistent with $T_{ion} = 13.2$ keV, inferred from the DT-n spectrum; red curve). A hint of the TT alphas can be seen in the energy range 1.5–2.5 MeV, but the DT alphas dominate the spectrum as expected for this shot with ~1.5% residual deuterium impurity in the fuel. Instrument design prevents detection in the gap in the energy range 2.5–2.8 MeV.

As expected, the 1.0 ns square pulse shape leads to upshifted DT-α spectra due to capsule charging, and the 2 ns ramped pulse shape gives downshifted DT-α spectra due to higher total implosion ρR (Fig. 6). The mean DT alpha energy (E_α) for the 0.6 ns square pulse shape case comes in very close to nominal, with a downshift consistent with $\rho R \lesssim 1$ mg/cm^2 ($\rho R = 0.4$ mg/cm^2 if we assume[18] $T_e = 1$ keV, $n_i = 10^{22}$/cm^3 and stopping in SiO_2 only for the most ranged down out of the three shots of this type, with $E_\alpha = 3.45$ MeV). The optimal pulse shape for charged-particle measurements is clearly the 0.6 ns square.

Another interesting question to consider in this context is the symmetry of the charged particle emission. It has been demonstrated[30] that variations in charged-particle yields measured in different locations around the target chamber are also reduced when the bang time is after the end of the laser pulse. Since alpha particle yields can only be measured in two locations on OMEGA, T^3He shot 73598 with similar implosion parameters as for the TT shots discussed above (OD = 981 μm, $\Delta t = 3.0$ μm, 16.6 kJ laser energy, SG0604, $P_{T2} = 3.5$ atm, $P_{3He} = 7$ atm, D impurity ~2%) was chosen for this demonstration. D^3He-proton yields from this shot measured in five different locations around the target chamber using the magnetic recoil spectrometer[31] (MRS), CPS and wedge range filter[32] (WRF) proton spectrometers are plotted in Fig. 7. Yield variations both globally and locally are seen to be insignificant within error bars. The standard deviation of all detectors is ~10%, while a weighted average yield of $3.3 \times 10^9 \pm 3.2\%$ (Ref. 33) is inferred from the ensemble of measurements.

The indication from all measurements described above is that these implosions are reasonably 1D in nature. This is further supported by time-integrated x-ray images of these implosions, which indicate that the implosions are highly spherical.

We conclude that an OMEGA platform to measure charged-particle yields and spectra from reactions relevant to SN and BBN has been successfully developed. The platform has already been exploited to measure the rate of the T^3He-γ reaction, ruling this reaction out as an explanation for the ^{6}Li abundance problem;[11] to measure an energy-dependence of the T(t,2n)α reaction at center-of-mass energies from 16 to 50 keV;[34] and for initial studies of the proton spectra from the ^{3}He(^{3}He,2p)α and T(^{3}He,np)α reactions.[12]

IV. NIF EXPERIMENT DESIGN

The laser energy and power available on NIF (max 1.8 MJ, 500 TW) are much higher than at OMEGA (max 30 kJ, 30 TW). This allows NIF to generate larger plasma volumes compared with OMEGA, which enables experiments with equivalent yield, and thus similar data quality, at lower temperature and, hence, conditions more directly relevant to

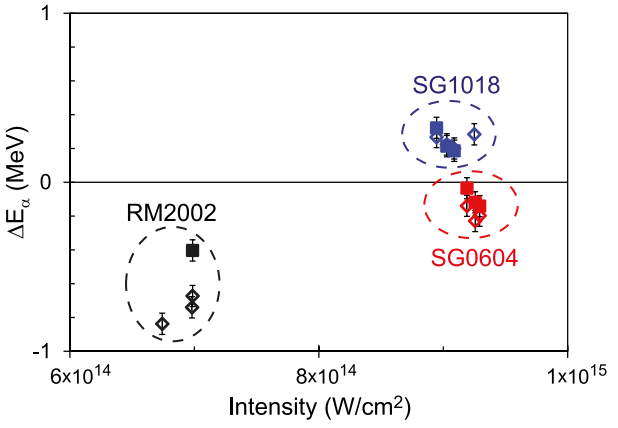

FIG. 6. Measured mean DT alpha energy relative to nominal for the different pulse shape cases (the nominal energy is corrected for upshifts due to finite T_{ion} as in Ref. 28). Hollow diamonds represent CPS2 data, solid squares CPS1. Blue symbols represent shots where the SG1018 laser pulse was used (bang time during the laser pulse), red symbols shots where the SG0604 laser pulse was used (bang time after the laser pulse), and black symbols shots where the RM2002 laser pulse was used (bang time during the laser pulse; higher areal density).

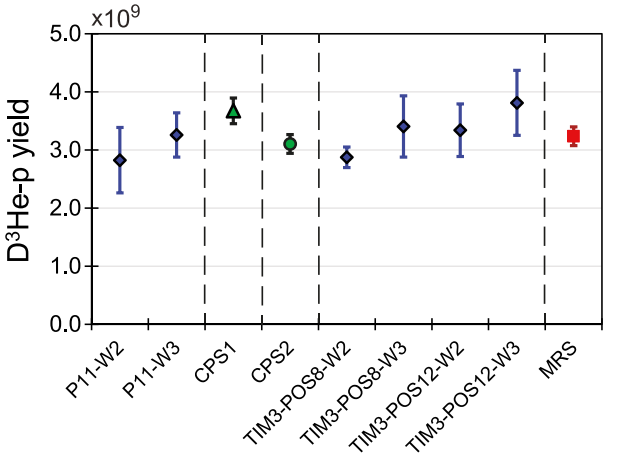

FIG. 7. D^3He proton yields measured in nine locations around the OMEGA target chamber for 50:50 T^3He shot 73598 (with ~2% D impurity in the fuel). Blue diamonds represent WRF data, the red square MRS data, the green triangle CPS1, and the green circle CPS2. The two WRF modules in the P11 port are only about 2 cm apart, and the four modules in TIM3 are within ~10 cm^2. CPS1, CPS2, MRS, P11, and TIM3 are distributed around the chamber at polar, azimuthal angles of $\theta,\varphi = 63°,198°$, $\theta,\varphi = 37°,18°$, $\theta,\varphi = 119°,308°$, $\theta,\varphi = 117°,234°$, and $\theta,\varphi = 143°,342°$, respectively. Yield variations both globally and locally are seen to be insignificant within error bars.

SN. As an aside, note that much higher densities can also be achieved at NIF than at OMEGA, as evidenced by the record areal densities obtained at the two facilities of $\sim$1.3 g/cm^2 at NIF[10] and $\sim$0.3 g/cm^2 at OMEGA.[35] This higher density presents a significant advantage when attempting to obtain high yield at low T_{ion} when studying neutron- or gamma-producing SN-relevant reactions the probing of which does not require low ρR. However, since the focus of this paper is on measurements of charged-particle producing reactions, this will not be further discussed here.

A glass-shell "exploding pusher" platform for implosions on the NIF was initially developed to calibrate the NIF nuclear diagnostic suite.[36–40] D_2, D_2/^{3}He and DT-gas-filled capsules were imploded using this platform from 2010 through 2014, with the primary goal of generating a large amount of neutrons and protons at low areal density for diagnostic calibration purposes. With varying drive conditions, these early implosions (OD $\sim$ 1600 μm, $\Delta t \sim 4.5$ μm) achieved DD T_{ion} ranging from 4.0 keV (for NIF shot N130129) to 11.3 keV (for NIF shot N120328), DD-neutron yields up to $\sim 10^{12}$ and acceptably low total ρR's ($\lesssim$10 mg/cm^2) in some cases, with laser energies varying from 43–131 kJ.[38] Based on reactivity scaling, i.e., using the reactivities from Fig. 1(b) and assuming the same burn conditions (density and T_{ion}) as for these reference implosions but pure ^{3}He fuel instead of D_2, a ^{3}He(^{3}He,2p)α proton yield of $\sim 3 \times 10^7$ should be achievable at $T_{ion} = 11$ keV. A yield of $\sim 5 \times 10^6$ is estimated to be required for a strong spectral measurement of this reaction on the NIF. Given this, a set of three implosions with ^{3}He, T_2 and 50:50 T_2/^{3}He fills at the same initial density ($\sim$1.4 mg/cm^3) was designed, based on reference shot N120328, as a first platform development experiment to make SN-relevant measurements on NIF. Note that these capsules have OD $\sim$1600 μm, which nominally gives only $\sim$4$\times$ increase in burn volume compared to the OD $\sim$ 1000 μm capsules used on OMEGA, but these experiments use less than 1/10th of the total laser energy available on NIF and it should be possible to push to much larger capsules in future experiments.

NIF presents the additional challenge over OMEGA that the beam configuration is optimized for indirect drive, with the 192 available laser beams divided in four upper and lower cones at 23.5°, 30°, 44.5°, and 50° angles to the polar axis, respectively. Hence, the targets have to be driven with polar-direct drive (PDD),[41] which makes it challenging to achieve a symmetric implosion. We attempt to accomplish this by designing a scheme for re-pointing the beams around the target for uniform illumination using the SAGE code[42] and the method described in Ref. 26. This has been shown to work well in PDD experiments with thicker CH shells,[43,44] and has also been used to design pointings for earlier NIF PDD exploding pusher implosions, including N120328.[37] Time-resolved x-ray images obtained on reference shot N120328 showed a fairly substantial non-uniformity with the implosion being oblate (diameter $\sim$940 μm $\times$ 800 μm) in-flight at t = 1.14 ns, even though SAGE simulations indicated that the implosion should be symmetric. For this reason, a new pointing design was developed for these implosions that according to SAGE would over-drive the capsule on the equator, compensating for the observed asymmetry on N120328 (Fig. 8). In this design, all beams were at best focus, and all beams had the same energy. All 50° beams and the lower ring of 44.5° beams were pointed close to the equator. Within each set of four grouped beams (quad), two beams were shifted to the left and two to the right for improved azimuthal uniformity.

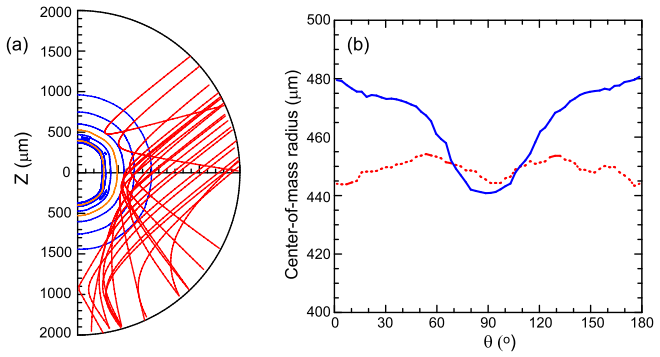

FIG. 8. (a) SAGE density contour plot from a run with the beam pointing that was selected for the first round of NIF platform development shots. The orange lines represent the critical density n_c, and the contours outside the outer orange line $n_c/2$, $n_c/4$, and $n_c/8$, respectively. Also shown is a subset of rays from a 50° beam. Note that the beam is repointed to below the equator of the target. (b) A comparison between the center-of-mass radius at 1.6 ns (in-flight) as a function of polar angle θ for two different runs. SAGE predicted that the best symmetry would be obtained with the pointing design shown in red (dashed curve), but based on earlier experience, the pointing design shown in blue (solid curve) with a predicted over-drive on the equator was selected for the experiment.

V. NIF EXPERIMENT RESULTS

Table II summarizes implosion parameters for the first set of NIF nuclear astrophysics platform development shots as well as for reference shot N120328. The goals of these shots were to study and compare the broad energy spectra of particles from the complementary six-nucleon-systems T(t,2n)α, ^{3}He(^{3}He,2p)α, and T(^{3}He,np)α, and to compare the many measurable nuclear yields from these three implosions[12] to assess the achievable accuracy in ^{3}He^{3}He stellar rate measurements using this platform. The energy spectra from these few-body reactions are interesting from a fundamental nuclear physics point of view; the mechanisms governing these reactions are not well understood. The spectral data will be used to benchmark theory for the spectral shape of the 3-body final-state spectra, both R-matrix[16,45,46] and *ab-initio*.[47,48]

Note that the implosion parameters within the set of new shots are very similar (except for the variations in fill). Compared to the reference shot, there are a few important differences: (i) the laser energy delivered is higher on the reference shot by $\sim$15% (although the same 125 kJ laser energy was requested on all four shots), (ii) the capsule wall is thinner on the reference shot by $\sim$0.3 μm, and (iii) the fill pressure is higher by nearly 2$\times$ (although the density is not that different, because of the lower deuterium mass).

The ramped laser pulse shape used on these implosions (including on N120328) is shown in Fig. 9 together with the x-ray burn history as measured by SPIDER[49] and the DT-n bang time as measured by MagPTOF[49] for shot N160530–001. The x-ray emission is filtered through 10.58 μm Ge ($h\nu \gtrsim 4$ keV); the narrow peak with FWHM $\sim$ 200 ps is expected to correspond to the core burn, while the broader feature below

TABLE II. Parameters of the 3 first NIF platform development shots with the goal of studying reactions relevant to stellar nucleosynthesis. Values for reference shot N120328[38] are also shown. (N_k is the Knudsen number, which is discussed in more detail in Section VII).

Shot	Pulse length (ns)	Laser energy (kJ)	Capsule diameter (μm)	Shell thickness (μm)	T2 fill pressure (atm)	^{3}He fill pressure (atm)	Initial density (mg/cm^3)	x-ray bang time[a] (ns)	N_k
N160530-001	2.1	113.0	1578	4.7	5.2	…	1.30	2.05 ± 0.03	0.3
N160601-001	2.1	113.6	1579	4.7	…	11.04	1.39	2.02 ± 0.03	0.01
N160601-002	2.1	111.3	1594	4.6	2.65	5.98	1.42	2.07 ± 0.03	0.05
N120328 (ref)	*2.1*	*130.6*	*1555*	*4.4*	*9.9 atm D_2*		*1.66*	*1.77*	*0.3*

[a]Measured using the SPIDER[73] x-ray detector.

(FWHM ∼ 800 ps) is expected to be due to SiO_2 x-ray emission. Note that bang times are observed (marginally) after the end of the laser pulse for these implosions.

Tables III–V summarize predicted and measured yields and T_{ion} for the first set of three NIF shots. Only yields from reactions between the primary fill species are included in the tables; in addition, a DT-n yield is measured for the T_2-filled implosion, a D^3He-p yield for the ^{3}He-filled implosion, and DT-n and D^3He-p yields for the T_2/^{3}He-filled implosion, but these cannot be directly compared to predictions at this point because the deuterium content is not well known (see Appendix B). The TT-n yield and burn-averaged DT T_{ion} for the T_2 and T_2/^{3}He implosions are measured using nTOF detectors 18–22 m from the implosion.[50,51] The T^3He-deuteron yield is measured using the MRS[52] and step-range-filter (SRF) detectors.[53] For the ^{3}He-filled implosion, the ^{3}He^{3}He yield and the D^3He-proton spectrum are measured using WRF proton spectrometers[54] fielded 10 cm from TCC (T_{ion} for this shot is estimated from the width of the D^3He-p peak). The 1D free-fall yield is inferred from a free-fall analysis[55] of pre-shot 1D ARES simulations (the free-fall analysis is intended to compensate for 2D effects leading to a decrease in yield relative to 1D for these PDD implosions). The scaled yield comes from reactivity scaling from reference shot N120328 corrected for 1D-LILAC[56]-simulated expected performance increases when going from a 9.9 atm to a 5.2 atm fill and from a 4.4 μm to 4.7 μm thick shell (according to the 1D simulations, these two changes should boost the yield by ∼25% and ∼5%, respectively).

It is clear from studying Tables III–V that the yields for these implosions came in lower than predicted. This can largely be explained by the lower-than-expected T_{ion}. The reactivity for the TT reaction is about 2.2 times higher at 11 keV than at 8.2 keV (Fig. 1(b)), which means that the entire difference between the TT-n yield predicted based on reactivity scaling from D_2 reference shot N120328 and the TT-n yield measured on N160530-001 can be explained by the T_{ion} difference between the two shots. Similarly, the reactivity for the ^{3}He^{3}He reaction is about 155 times higher at 11 keV than at the very roughly estimated T_{ion} for shot N160601-001 of 6 keV. This would also be more than enough to explain the difference between the predicted and measured ^{3}He^{3}He-p yields. However, the TT reactivity ratio

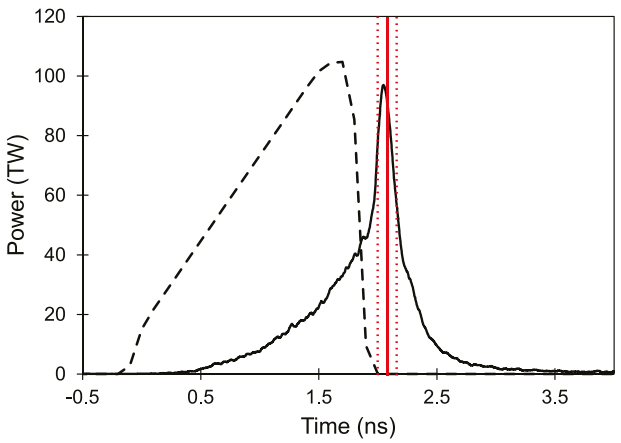

FIG. 9. Delivered laser power as a function of time for NIF shot N160530-001 (dashed black curve), shown together with SPIDER-measured x-ray emission history (solid black curve, a.u.). An x-ray bang-time of 2.05 ± 0.03 is inferred from the SPIDER data from this shot. Also shown is the DT-n bang-time inferred from the MagPTOF detector (solid red line), with the dashed red lines representing the uncertainty in this measurement.

TABLE III. Measured and predicted TT-n yield and DT T_{ion} for T_2-only NIF shot N160530-001. DT T_{ion} is inferred from the width of the DT-n spectrum and can be measured because of a small deuterium impurity in the T_2 fill (∼0.15% by atom). The 1D free-fall yield comes from a free-fall analysis of pre-shot 1D ARES simulations. The scaled yield is based on reactivity scaling from reference shot N120328.

N160530-001	TT-n yield	DT T_{ion} (keV)
1D free-fall	1.1×10^{13}	
Scaled	1.7×10^{12}	11
Measured	$(8.2 \pm 1.7) \times 10^{11}$	8.2 ± 0.2

TABLE IV. Measured and predicted ^{3}He^{3}He-proton yield and estimated T_{ion} (inferred from the width of measured D^3He-proton spectra) for ^{3}He-fill NIF shot N160601-001. The same comments as for Table III apply.

N160601-001	^{3}He^{3}He-p yield	T_{ion} (keV)
1D free-fall	2.8×10^9	
Scaled	3.8×10^7	11
Measured	$\sim 4.1 \times 10^5$	∼6

TABLE V. Measured and predicted TT-n and T^3He-deuteron yields and DT T_{ion} for mixed T_2/^{3}He-fill NIF shot N160601-002. The same comments as for Table III apply.

N160601-002	TT-n yield	T^3He-d yield	DT T_{ion} (keV)
1D free-fall	1.5×10^{12}	8×10^{10}	
Scaled	4.2×10^{11}	6.7×10^9	11
Measured	$(6.9 \pm 1.4) \times 10^{10}$	$(4.5 \pm 0.1) \times 10^8$	7.1 ± 0.2

going from 11 keV to 7.1 keV of 3.4 is not enough to explain the difference between the predicted and observed TT-n yields for shot N160601-002 (a factor 6.1). The T^3He reactivity ratio going from 11 keV to 7.1 keV of 7.9 is also not enough to explain the difference between predicted and observed T^3He-d yields (a factor 15). Some additional factor appears to be degrading the performance of the $T_2/^3He$-mixed-fill shot relative to the reference shot.

When using the measured T_{ion} to scale yields using the reactivities from Fig. 1(b), it is important to keep in mind that T_{ion} as inferred from the neutron spectrum[28] may also be affected by flows in the implosion[57–59] (this is further discussed in Section VI below). In this context, it is interesting to compare T_{ion} as measured by four different nTOF detectors in different locations around the NIF target chamber (Fig. 10). For the $T_2/^3He$-mix shot, DT T_{ion} measured in three different lines of sight distributed from 8° to 116° polar angle is seen to agree very well with each other ($\chi^2_{red} = 0.1$). For the T_2-only shot on the other hand, DT T_{ion} measured in four different lines of sight distributed from 8° to 161° polar angle shows signs of anisotropy ($\chi^2_{red} = 1.8$), with higher T_{ion} being inferred near the equator, which may indicate flow broadening of the DT-n peak.

Time-resolved self-emission x-ray imaging[60] was used to diagnose symmetry for these implosions. Fig. 11 shows an in-flight ($t \sim 1.75$ ns) x-ray image from an equatorial view (polar, azimuthal angles $\theta,\varphi = 90°,78°$) for shot N160530-001. The implosion is strongly oblate at this time, with an equator-to-pole aspect ratio of ~1.5 (diameter $\sim 610 \times 400\ \mu m$), indicating that the laser drive is significantly stronger on the pole than on the equator and that more work is required to optimize the laser drive uniformity for these implosions. The asymmetry persists through burn, as confirmed by self-emission images taken around bang time for all three implosions (Fig. 12). Note that while the equatorial images (upper row in Fig. 12) consistently appear very oblate, the polar images (lower row in Fig. 12) are nearly round. This is consistent with the beam symmetry on NIF. A burn volume of 5×10^{-3} mm^3 is estimated from the N160601-001 data.

An all-important question in terms of the goals of these shots concerns the symmetry and level of distortion of charged-particle fusion products emitted from the implosions.

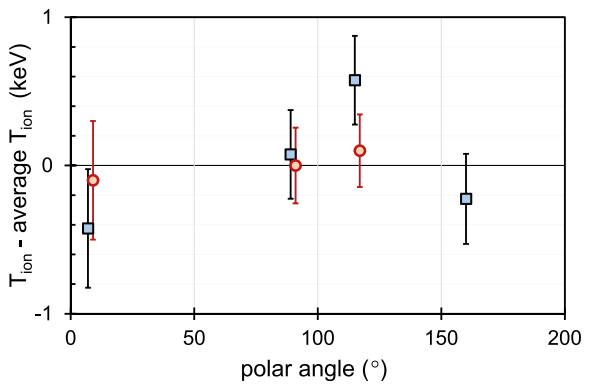

FIG. 10. DT T_{ion} as measured by individual NIF nTOF detectors minus the average of all reporting detectors for the T_2-only shot (squares) and the T^3He-mix shot (circles), plotted as a function of the detector polar angle. (The points are artificially separated in polar angle for clarity.)

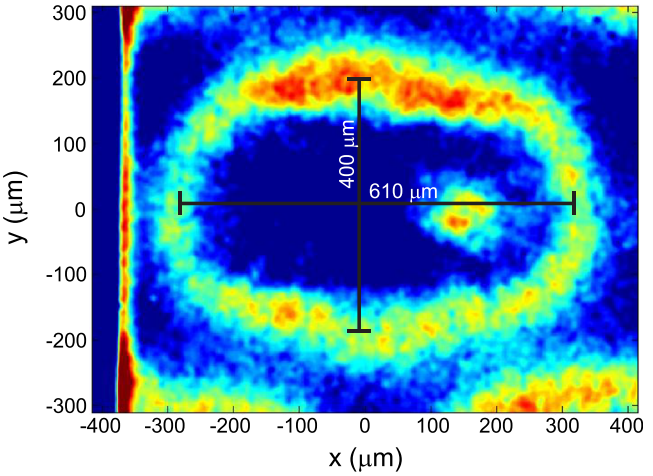

FIG. 11. In-flight ($t = 1.75$ ns) x-ray image from an equatorial view ($\theta,\varphi = 90°,78°$) for T_2-only NIF shot N160530-001. The color scale represents x-ray intensity originating from the SiO_2 shell.

Fig. 13 shows the D^3He-p yields measured in different locations around the target chamber on $T_2/^3He$-mix shot N160601-002, using the MRS, WRF, and SRF detectors. MRS is located at polar, azimuthal angles $\theta,\varphi = 73°,324°$ and the WRF and SRF detectors are held by three diagnostic-insertion modules (DIM) at $\theta,\varphi = 0°,0°$, $\theta,\varphi = 90°,78°$ and $\theta,\varphi = 90°,315°$, respectively. (The SRF and WRF modules connect to each DIM at ±13° and ±3.5° from the DIM axis.) Note that while the MRS and WRF detectors give an average yield value in their respective lines of sight, the SRFs are flat-filter detectors each covering a 5 cm-diameter round area at ~50 cm from TCC (~0.01 sr), and thus allow study of local variations in D^3He-p fluence. The black error bars in Fig. 13 span the range from maximum to minimum yield inferred across a single SRF module. This shows that local yield variations are as large as or larger than global yield variations observed between the MRS and the three DIMs. The standard deviation of all measurements is ~12%, which is a bit high for an implosion with bang-time after the end of the laser pulse.[30] Using all 12 samples, the total D^3He-p yield from the implosion is constrained to $2.7 \times 10^8 \pm 8.5\%$.[61] This total uncertainty is higher than observed on a similar, smaller scale implosion on OMEGA (Fig. 7). Anisotropies in fluence around the implosion result from deflections in electromagnetic fields, the topology of which can be expected to be impacted by the symmetry of the implosion. The current hypothesis is that reduced asymmetry in the implosion will also reduce yield fluctuations.

In Fig. 14, D^3He-proton energy spectra measured in different locations around the implosion are compared to the nominal expected D^3He-p spectrum (dashed line, calculated assuming $T_{ion} = 7.1$ keV, $Y_{D3Hep} = 2.7 \times 10^8$, and an instrument resolution of 159 keV). The average spectrum measured by the two WRFs on the pole (red curve) compares well with the nominal spectrum, with only minor distortion and a ~0.15 MeV downshift, indicating little ρR on the pole. Spectra measured closer to the equator (MRS in gray, average of equatorial WRFs in black) show substantially more distortion with a significant low-energy tail, and are also noticeably more downshifted than the polar spectrum. This

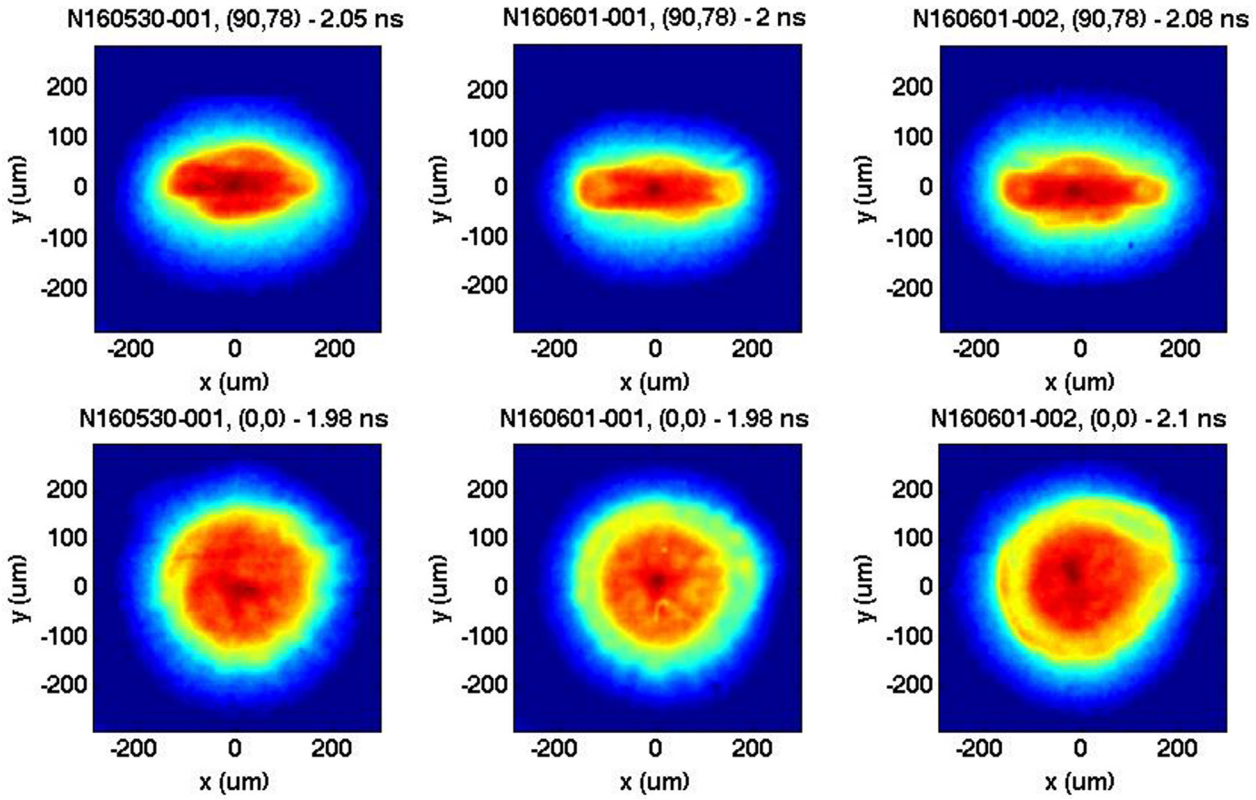

FIG. 12. Core x-ray images from the first round of three NIF shots (N160530-001, N160601-001, and N160601-002). The upper row shows the implosions as viewed from the equator ($\theta,\varphi = 90°,78°$), while the lower row represents the view from the north pole ($\theta,\varphi = 0°,0°$). All three implosions behave very similarly. While they look nearly round as viewed from the pole, they are substantially oblate as viewed from the equator, indicating a relatively lower laser drive in the equatorial plane. (The deviation from round in the top right corner of the polar data is in the same direction as the stalk that holds the target, and is most likely caused by this engineering feature.)

indicates more ρR at burn on the equator than on the pole, and also ρR evolution during the time ($\sim$200 ps) of nuclear emission. The difference between polar and equatorial spectra provides further evidence of the poor implosion symmetry perturbing the measurements. Note, however, that while evident, the spectral distortions are relatively minor. This result bodes well for accurate charged-particle spectral measurements at negligible ρR in future further optimized NIF implosions.

Scattered light measurements were also made on these shots and will help constrain future pointing designs. Analysis of these data is in progress.

We conclude that while significant progress has been made towards developing a platform for study of charged-particle-producing reactions relevant to SN and BBN on the NIF, some further work is required before it is fully optimized (see Section VII).

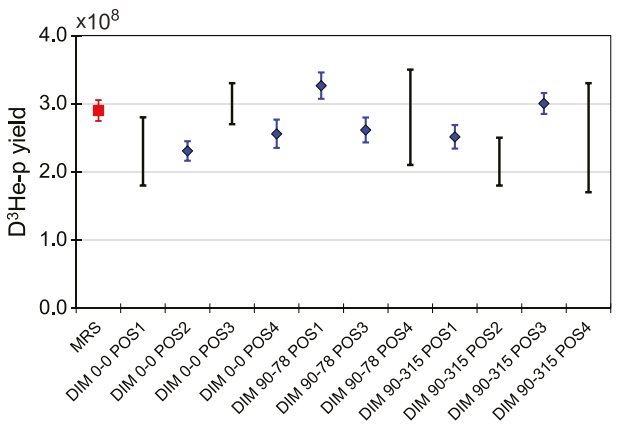

FIG. 13. D^3He-p yields measured in 12 different locations around the NIF target chamber on $T_2/^3He$-mixed-fill shot N160601-002. The red square represents MRS at $\theta,\varphi = 73°,324°$, black error bars SRF data, and blue diamonds WRF data. The three diagnostic insertion modules (DIM) used to hold the WRF and SRF detectors are located at $\theta,\varphi = 0°,0°$, $\theta,\varphi = 90°,78°$ and $\theta,\varphi = 90°,315°$, respectively.

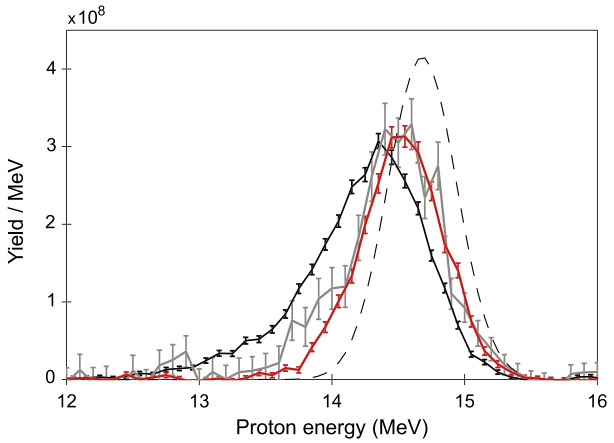

FIG. 14. D^3He-p spectra as measured on the pole (average for DIM 0°,0° WRF positions; red), on the equator (average for 90°,78° and 90°,315° WRF positions; black) and 17° above the equator (MRS, gray). Also shown is the nominal expected spectrum (dashed curve), assuming $T_{ion} = 7.1$ keV, $Y_{D3Hep} = 2.7 \times 10^8$, an instrument resolution of 159 keV and considering temperature-dependent upshift.[28]

VI. CENTER-OF-MASS ENERGY CONSIDERATIONS

An essential aspect of any astrophysically relevant nuclear experiments is understanding the conditions at which the reactions are probed. As in a star but unlike in an accelerator experiment, reactions are not probed at a single center-of-mass (c-m) energy in an ICF implosion. The fuel ions are expected to follow a Maxwellian (or similar modified[62,63]) energy distribution characterized by the plasma T_{ion}. Because the Coulomb barrier penetrability scales very strongly with energy, it is primarily the ions in the highly energetic tail of the distribution that will undergo reactions. The effective c-m energy distribution of the reacting ions is described by the Gamow peak.[1]

In this context, it should be considered that while current ICF nuclear diagnostics measure a single burn-averaged T_{ion}, the temperature and density in an ICF implosion are never homogeneous throughout. The details of the distributions will vary depending on implosion design. Fig. 15 shows example T_{ion} and density distributions simulated using the 1D radiation hydrodynamics code HYADES[64] for an OMEGA-scale, 1000-μm OD, 3.0-μm thick SiO_2-shell implosion with 9 atm T_2 fill shot with a 30 kJ, 0.6 ns square laser pulse, and using LILAC for a NIF-scale, 1600-μm OD, 4.0-μm thick SiO_2-shell implosion with 5.2 atm T_2 fill shot with a 70 kJ, 1.2 ns ramped laser pulse (burn duration from this simulation is ~70 ps, total $\rho R = 10$ mg/cm^2).

As discussed in Ref. 65, because of the different temperature dependence of the reactivities for the various reactions of interest (Fig. 1(b)), variations in T_{ion} and density throughout the implosion can lead to different burn-weighted T_{ion} for the different reactions. Using the fact that the yield from any one fuel element with constant density and temperature and volume V scales as $Y \sim n_i n_j \times \langle \sigma v(T_{ion}) \rangle_{ij} \times V$, we can calculate burn-averaged temperatures from the various reactions using the profiles from Fig. 15 (under the assumption that they are constant as a function of time). To make a realistic comparison to experimental results, we scale the T_{ion} profiles from Fig. 15 down to match DT T_{ion} measured on the OMEGA and NIF shots. For the OMEGA profiles (Fig. 15(a)) with T_{ion} scaled by a factor 0.727, this gives calculated burn-averaged DT $T_{ion} = 13.30$ keV, TT $T_{ion} = 13.32$ keV, T^{3}He $T_{ion} = 13.45$ keV, D^{3}He $T_{ion} = 13.46$ keV, and ^{3}He^{3}He $T_{ion} = 13.67$ keV. For the NIF profiles (Fig. 15(b)) with T_{ion} scaled by a factor 0.427, this gives calculated burn-averaged DT $T_{ion} = 8.22$ keV, TT $T_{ion} = 8.22$ keV, T^{3}He $T_{ion} = 8.67$ keV, D^{3}He $T_{ion} = 8.66$ keV, and ^{3}He^{3}He $T_{ion} = 9.09$ keV. Clearly, assuming that the simulations accurately describe what is actually achieved in the experiments, differences in burn-averaged T_{ion} between these reactions for this type of implosion with relatively flat T_{ion} and density profiles are expected to be small.

The mean energy and width of the Gamow peak scale as $T_{ion}^{2/3}$ and $T_{ion}^{5/6}$, respectively.[1] Hence, the c-m energy distribution at which reactions are probed will vary along with T_{ion} throughout the implosion. A burn-weighted Gamow-peak can be calculated similarly to the burn-weighted T_{ion} for different reactions above, by weighting the distribution in each volume element by the yield expected to be produced in that volume element. In Fig. 16, Gamow peaks calculated using the single, burn-weighted T_{ion} for the scaled OMEGA and NIF simulations from Fig. 15 (TT $T_{ion} = 8.22$ keV and TT $T_{ion} = 13.32$ keV, respectively) are contrasted to such burn-weighted Gamow-peaks for the two scaled simulations. A slight difference is observed between the burn-weighted Gamow-peak and the Gamow-peak calculated using the burn-averaged T_{ion} for the NIF simulation with ~2× variation in T_{ion} across the burn region, while virtually no difference can be seen for the OMEGA simulation with <20%

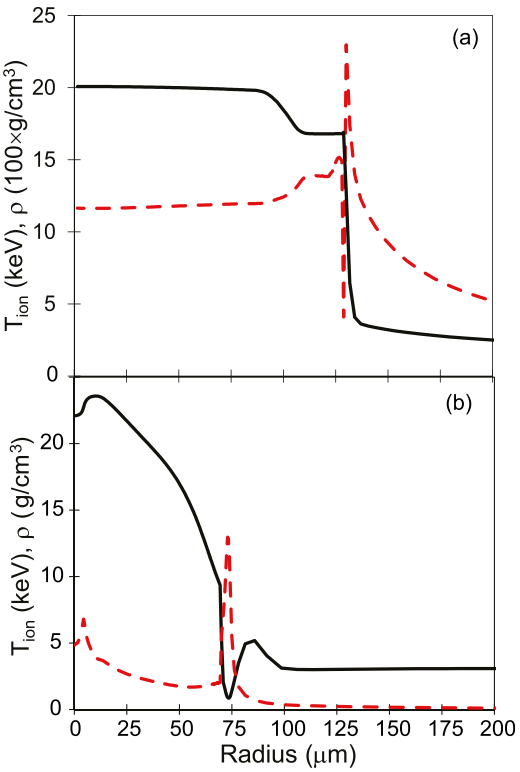

FIG. 15. Radial temperature (solid black curve) and density (dashed red curve) profiles calculated using (a) 1D HYADES simulations for an OMEGA-scale implosion and (b) 1D LILAC simulations for a NIF-scale implosion (see text for details). The fuel-shell interface is at ~128 μm for the OMEGA-scale implosion and ~69 μm for the NIF-scale implosion.

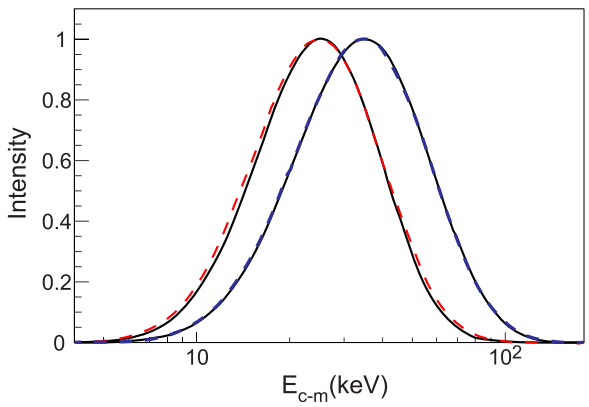

FIG. 16. Gamow-peak energy distributions calculated for the TT reaction using a single, burn-averaged TT T_{ion} (solid curves) contrasted to effective burn-weighted Gamow-peak energy distributions calculated using the radial profiles in Fig. 15 (dashed curves, with T_{ion} scaled down to match T_{ion} measured on NIF and OMEGA). The left two peaks are for the NIF case (TT $T_{ion} = 8.2$ keV) and the right two peaks for the OMEGA case (TT $T_{ion} = 13.3$ keV).

variation in T_{ion} across the burn region. This result lends confidence that the conditions at which the reactions are probed are sufficiently well understood.

Since T_{ion} is inferred from the width of fusion product spectra[28] from ICF implosions, other factors than variations in T_{ion} throughout an implosion may also impact the measured, burn-weighted T_{ion}.[60] As mentioned in Section V above, an important such factor is directional fuel motion (flow) during burn, which may lead to additional, non-thermal broadening of fusion product spectra.[58,59] If the burning fuel assembly is moving in a single direction, this will lead to a shift in the observed mean energy of fusion product spectra. Such an effect has been previously observed for PDD exploding pushers on NIF.[66] This effect will not impact the inferred T_{ion}, and thus not the ability to correctly infer the conditions at which a reaction is probed. If, on the other hand, different fuel elements are moving in different directions during burn (e.g., radial[59] or turbulent[58] motion), this will lead to additional, non-thermal peak broadening, which, if not considered, will result in an over-estimate of the plasma T_{ion}. Two different scenarios in which this could happen can be imagined for our exploding pusher-type implosions: 1D motion, in which case burn happens while the fuel is moving radially, or 3D motion, in which asymmetries in the implosion seed non-uniform flows. For the 1D case, the inferred T_{ion} would be uniformly inflated around the implosion, while for the 3D case, variations in the inferred T_{ion} could be expected around the implosion. The impact of 3D flow can be studied by measuring T_{ion} in different lines of sight. As can be seen in Fig. 10, a line-of-sight difference of 1.0 ± 0.5 keV was observed for NIF shot N160530-001, while no difference outside of the error bars was seen for the nearly identical shot N160601-002. At first glance, these results do not conclusively answer the question about the impact of 3D flow. The goal for future experiments is to reduce implosion asymmetry, hence eliminating 3D flow as a factor.

The impact of 1D radial flow was assessed using post-shot 1D ARES simulations attempting to match data from six earlier NIF exploding pusher shots, including N120328. These simulations indicated flow-enhancement of T_{ion} ranging from 0.2 to 1.7 keV for the six implosions, using a reaction-weighted average implosion velocity to estimate the flow broadening[58] (we note that this quick estimate gives a slightly higher value compared to the more accurate treatment of including the impact of flow on neutron spectra from each fuel element and inferring T_{ion} from the total final spectrum). This corresponds to reaction-weighted implosion velocity variances ranging from 90–310 km/s. Note, however, that the simulations were struggling to match measured T_{ions} for these implosions, and that they are inherently limited in that they are 1D approximations of a highly 2D (or 3D) problem.

VII. DISCUSSION AND FUTURE DIRECTIONS

In this paper, the development of robust HED platforms for probing astrophysically relevant charged-particle-producing nuclear reactions on OMEGA and the NIF has been described. On OMEGA, the platform is fairly mature, with the first physics results already published[11] and more in the pipeline.[12,34] On the NIF, significant progress has been made, but some further work is required. First and foremost, the symmetry of NIF implosions must be improved to ensure reliable charged-particle measurements. Improved symmetry is also expected to contribute more generally to enhanced implosion performance. As discussed, achieving symmetry is challenging because of the NIF beam geometry. Several avenues are being pursued to learning how to improve laser drive uniformity for these implosions. First, output from SAGE simulations is being compared to symmetry results from earlier implosions, with the goal of finding a way to adjust the design for improved pointing. For the next round of NIF implosions, differential beam energies with relatively higher laser energy in the beams pointed towards the equator will be implemented in addition to beam repointing. In parallel, 2D simulations using the radiation hydrodynamics codes ARES, HYDRA,[67] and DRACO[68] are also being developed to address pointing optimization. In particular, we conjecture that cross-beam energy transfer (CBET) as the implosion converges contributes to the pointing challenges—this will be addressed using DRACO, which includes a CBET package.

The first round of implosions on the NIF also produced lower than desired yields; in particular, the ^{3}He^{3}He-p yield generated was too low for a high-quality measurement of the ^{3}He^{3}He proton spectrum. Comparing the data with results from reference implosions such as N120328 leads to the conclusion that yields were low primarily due to lower-than-expected T_{ion} for these initial NIF experiments. The most direct way to obtain higher T_{ion} for these implosions is to increase the laser energy delivered to the target. Fig. 17 shows the predicted increase in T_{ion} as a function of absorbed laser energy from a 1D free-fall analysis of 1D ARES simulations of a NIF-scale implosion with OD = 1600 μm, shell thickness 4.5 μm, $P_{T2} = 5.2$ atm and using a 2.1 ns ramped laser pulse shape. Note that the difference in absorbed laser energy according to these simulations would need to be ~22 kJ to go from the 11.3 keV T_{ion} observed on N120328 to the 8.2 keV T_{ion} observed on N160530-001. This does not seem unreasonable given that the difference in delivered laser energy between the two shots was ~18 kJ (Table II). However, note that the fraction of laser light that is actually

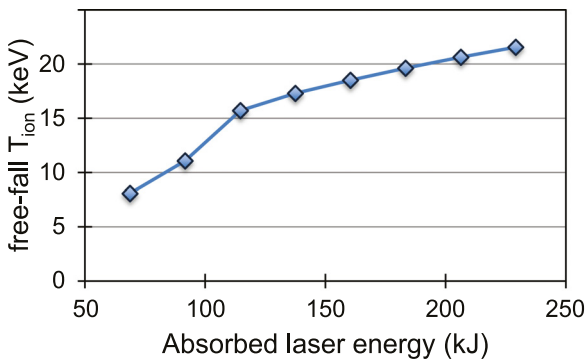

FIG. 17. Simulated TT T_{ion} as a function of absorbed laser energy from free-fall analysis of 1D ARES simulations of a NIF-scale implosion with OD = 1600 μm, shell thickness 4.5 μm, P = 5.2 atm T_2 and using a 2.1 ns ramped laser pulse shape.

absorbed by the capsule for one of these implosions (i.e., the translation factor needed to go from incident to absorbed laser energy, and hence allow direct comparison between measurements and simulations) is not well understood at present.

Longer term, the strategy is to increase the yield of NIF implosions at a set temperature by going to larger plasma volumes, thus more fully exploiting the laser energy available on the NIF. This will allow probing of SN-relevant reactions at more astrophysically germane temperatures. Design work for this effort is underway. It is expected that the laser energy would have to increase as capsule radius r^3 to achieve the same plasma conditions with progressively larger targets.[26] If this holds, ~16× more yield could be produced with a 4-mm OD capsule driven with 1.8 MJ than with a 1.6-mm OD capsule driven with 113 kJ.

A potential challenge that must be handled when inferring astrophysical rates from these relatively low-density implosions is any kinetic effects in the plasma that may be impacting implosion performance. Such effects could include:

(i) Tail ion loss, i.e., leakage of the highly energetic ions from the tail of the ion velocity distribution across the system boundary due to long mean free paths, as discussed theoretically in Refs. 62 and 63 and invoked to partially explain measurements in Refs. 9 and 38.
(ii) Anomalous diffusion leading to separation of the different ion species in a mixed-fill implosion, as discussed theoretically in Refs. 69 and 70 and invoked to explain data in Refs. 71 and 72.
(iii) Other multi-ion effects, such as ion thermal decoupling, invoked to explain data in Ref. 71.

Most detrimental to the efforts discussed in this paper would be any undiagnosed kinetic effects that change the relative yields between different reactions for cases where the rate of one reaction is to be inferred relative to the well-known rate of another. This has been shown to be a non-issue for denser, highly collisional implosions.[8] The question can also be circumvented by taking the ratio of one reaction branch to another, such as was done for T^3He-γ relative to T^3He-d in Ref. 11. Kinetic effects will also not impact our ability to make spectral measurements (although interpretation of the data could be complicated by kinetic effects, e.g., inasmuch as they impact the inference of plasma conditions such as T_{ion}). For the more general scenario of rate measurements from lower-density plasmas, however, this is a question that must be addressed. While this is still work in progress, a few initial observations can be made based on the OMEGA and NIF data presented in this paper.

Initial densities for the OMEGA implosions range from 0.8 mg/cm^3 for 77 951-77 952 to 2.4 mg/cm^3 for 67 941-68 448. Unfortunately, convergence was not measured for these implosions. Knudsen numbers (N_k) can be estimated by using simulated convergence ratios (CRs) from HYADES simulations of shots 77 951 (CR = 4.7), 77 960 (Fig. 15(a), CR = 3.8), and 77 963 (CR = 5.6) to be $N_k \sim 5$ for the low-gas-fill implosions (77 951–77 952), $N_k \sim 1$ for the high-gas-fill implosions driven by a 0.6 ns-square laser pulse, and $N_k \sim 0.1$ for the high-gas-fill implosions driven by a 2.0 ns ramped, de-focused laser pulse (simulated convergence numbers are not presently available for the 1.0 ns-square laser pulse case). Earlier work[38] has suggested that the yield drops to ~30% of clean simulated yield for $N_k \sim 0.3$ due to kinetic effects such as tail ion depletion, and that the reduction should be expected to be exacerbated with increasing N_k. Interestingly, ARES simulations of the high-gas-fill OMEGA implosions give an average TT yield-over-clean (YOC) of ~99% for the $N_k \sim 1$ implosions driven by a 0.6 ns-square laser pulse, and YOC ~ 93% for the implosions driven with the 1.0 ns-square laser pulse (see Section III). However, this remarkable result should be taken with a grain of salt because T_{ion} from the simulations (which were done pre-shot) came in a bit higher than measured (Fig. 2).

No simulations that reasonably well describe the NIF implosions exist at present. Available 1D simulations substantially over-predict T_{ion} for these highly asymmetric implosions, making any detailed YOC comparisons meaningless. 2D simulations using ARES, DRACO, and HYDRA are underway which can be expected to better capture implosion performance. Meanwhile, it is interesting as noted in Section V that performance for the pure T_2 and ^3He-filled shots, respectively, seems to scale as expected compared to the D_2-only reference shot N120328 when correcting for T_{ion}. This is in spite of N_k changing by more than an order of magnitude from 0.3 for the T_2 and D_2 shots to 0.01 for the ^3He-only shot (however, it may be questioned whether a global N_k calculation is meaningful for these highly asymmetric implosions). On the other hand, performance for the mixed-fill shot (T_2/^3He, $N_k \sim 0.05$) does not scale as expected compared to N120328. This might be an indication of multi-ion effects in the mixed fill. However, note that the T^3He-d and TT-n yield appear to be similarly impacted, which contradicts the hypothesis that anomalous diffusion between T and ^3He could be responsible for the observation.

VIII. CONCLUSIONS

An inertial-confinement-fusion platform using thin-glass-shell exploding pusher implosions to probe charged-particle-producing reactions relevant to SN and BBN has been developed on OMEGA. Optimized implosions with OD = 1000 μm and shell thickness 3.0 μm driven with a 0.6 ns square laser pulse are demonstrated to produce maximal yield at the necessary conditions to ensure that undistorted charged-particle spectra can be reliably measured, i.e., with negligible total ρR to minimize ranging in the assembled plasma, and bang time after the end of the laser pulse to prevent charged-particle energy upshifts due to capsule charging.

Development of a similar platform is in progress on the NIF, with the goal of leveraging NIF's higher capabilities in terms of laser energy and power to allow probing of astrophysically important reactions at more stellar-relevant conditions than at OMEGA. Initial NIF experiments struggle with symmetry due to NIF's indirect drive beam configuration. However, charged-particle data from the initial implosions look promising, and work is underway to address the symmetry problems.

Radial profiles from 1D radiation hydrodynamic simulations are invoked to show that variations in temperature and density throughout these thin-glass-shell exploding pusher implosions do not significantly impact our understanding of the conditions at which the reactions are probed. Future work includes further exploration of the impact of flows and kinetic effects in these types of implosions.

Lessons learned from these early proof-of-principle experiments will be used in studies of other astrophysically relevant reactions in the future. The long-term goal of this effort is to explore thermonuclear reaction rates and basic nuclear physics in stellar-relevant regimes not reachable through existing terrestrial experimental platforms.

ACKNOWLEDGMENTS

The authors would like to thank the OMEGA and NIF operations crews for executing these experiments, and Ernie Doeg, Robert Frankel, and Michelle Valadez for processing of the CR-39 data used in this work. This work was supported in part by DOE (DE-NA0001857, DE-NA0002905, DE-FG02-88ER40387), LBS, NLUF (DE-NA0002035), and LLE (415935-G).

APPENDIX A: TT YIELD MEASUREMENTS

Measurement of the TT yield presents a challenge for two reasons: (1) because of the broad energy spectrum of neutrons from the TT reactions, with the lowest energy neutrons not being detectable, and (2) because of previous poor understanding of instrument sensitivity in this energy range. As part of the first round of platform development shots on OMEGA, the TT yield was measured with four different diagnostics (Fig. 18) using three entirely independent methods with different systematics:

(a) A bibenzyl-scintillator-based nTOF detector 13.4 m from TCC, inferring the neutron spectrum from a time-of-flight measurement.

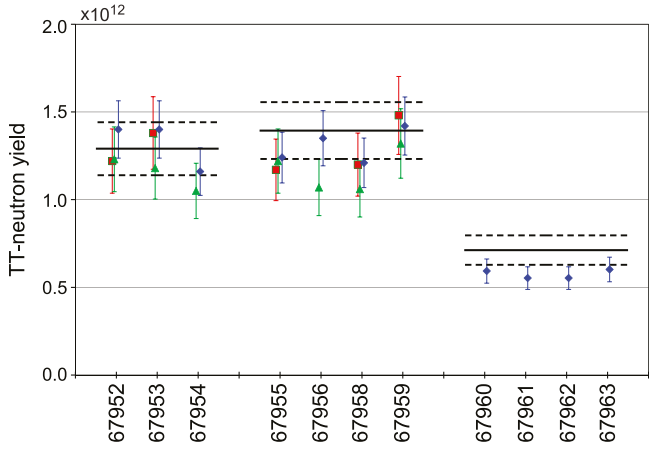

FIG. 18. TT neutron yields measured on the first round of platform development shots on OMEGA (Table I) using a bibenzyl nTOF detector (blue diamonds), the MRS neutron spectrometer (black solid lines), and indium (red squares) and aluminum (green triangles) activation, each of the latter two compared to copper activation to correct for DT neutrons. Note that the MRS integrated 3–4 shots per measurement, hence the broad lines which represent an average yield over the covered sets of shots. The dashed black lines represent the upper and lower uncertainty in the MRS measurement.

(b) A magnetic recoil spectrometer (MRS), inferring the neutron spectrum from measurements of recoil deuterons from elastic *n, d* scattering in a CD conversion foil momentum-separated in a magnet to end up in different physical locations in the detector depending on energy.

(c) Indium and aluminum activation measurements, each corrected for the contribution from DT neutrons using copper activation with activation threshold above the maximum TT neutron energy.

The four diagnostics were found to agree very well. This addresses point (2) above. Point (1) has so far been addressed primarily through R-matrix modeling,[45] benchmarked by recent measurements of the spectrum down to ∼2 MeV.[14] This work is still ongoing.

APPENDIX B: FILL CONSIDERATIONS

A significant challenge for the early experiments discussed in this paper has been to optimize the capsule fills. Because the reactivity for the DT and D^3He reference reactions are orders of magnitude higher than the reactivities for the T(t,2n)α, T(^{3}He,np)α, and ^{3}He(^{3}He,2p)α reactions (Fig. 1(b)), a primary goal has been to minimize the deuterium impurity in the fill. The level of deuterium impurity must also be extremely well known: relative yields between the reference reaction and the reaction under study can only be used to infer a reaction rate if the fuel composition is known, and any uncertainty in the fuel composition will translate directly to uncertainty in the inferred rate. This problem has not yet been fully solved for the T_2, ^{3}He or $T_2/^3$He fuel mixtures with trace deuterium for either OMEGA or NIF implosions.

SiO_2 capsules are filled using a diffusion method, with the capsules being placed in a manifold which is pressurized in stages up to the desired capsule fill pressure with time allowed for the fill to diffuse into the capsule at each stage. Diffusion rates at room temperature for these types of capsules are of order months to years for hydrogen isotopes, and of order hours to days for helium isotopes (the higher numbers are for capsules flash coated with a ∼0.1 μm Al barrier to reduce He leak rates). Hydrogenic fills (D_2, T_2) are done at high temperature (300 °C) to increase the diffusion rate of the capsules for manageable fill times (of order weeks). NIF capsules have to be flash coated with an Al barrier to prevent all the helium from leaking out of the capsule during the ∼8 h period between opening up a target pressure cell and imploding the target on NIF. For the NIF T_2 fills (expected D_2 impurity ∼0.1%–0.3%), the level of deuterium impurity has been evaluated by subjecting residual gas in the manifold post-fill to mass spectrometry. How representative these measurements are of what is actually in the capsule is being evaluated—to date, different experiments have had varying success in matching measured DT/TT yield ratios to estimated deuterium content. For OMEGA T_2 fills (expected D_2 impurity ∼1%–2%), assays of the fuel supply are used to estimate the deuterium impurity, and they have to be corrected for changes to the composition expected due to impurities being introduced in different stages of the fill cycle. For ^{3}He fills (expected D impurity ∼10–100 ppm), a method with crush tests of a witness capsule for each fill is being

developed to measure the impurity level. (In a crush test, a capsule filled as if to be shot is instead crushed in a manifold at high vacuum, and the gas released analyzed using a mass spectrometer to determine composition.) The crush test method will also be tried on future T_2/^{3}He mixed-fill shots at NIF.

[1]C. Iliadis, *Nuclear Physics of Stars*, 2nd ed. (Wiley-VCH Verlag GmbH & Co, Germany, 2015).

[2]T. R. Boehly, D. L. Brown, R. S. Craxton, R. L. Keck, J. P. Knauer, J. H. Kelly, T. J. Kessler, S. A. Kumpan, S. J. Loucks, S. A. Letzring, F. J. Marshall, R. L. McCrory, S. F. B. Morse, W. Seka, J. M. Soures, and C. P. Verdon, Opt. Commun. **133**, 495 (1997).

[3]B. M. Van Wonterghem, S. J. Brereton, R. F. Burr, P. Folta, D. L. Hardy, N. N. Jize, T. R. Kohut, T. A. Land, and B. T. Merritt, Fusion Sci. Technol. **69**, 452–469 (2016).

[4]C. A. Haynam, P. J. Wegner, J. M. Auerbach, M. W. Bowers, S. N. Dixit, G. V. Erbert, G. M. Heestand, M. A. Henesian, M. R. Hermann, K. S. Jancaitis, K. R. Manes, C. D. Marshall, N. C. Mehta, J. Menapace, E. Moses, J. R. Murray, M. C. Nostrand, C. D. Orth, R. Patterson, R. A. Sacks, M. J. Shaw, M. Spaeth, S. B. Sutton, W. H. Williams, C. C. Widmayer, R. K. White, S. T. Yang, and B. M. Van Wonterghem, Appl. Opt. **46**, 3276 (2007).

[5]M. Aliotta, F. Raiola, G. Gyürky, A. Formicola, R. Bonetti, C. Broggini, L. Campajola, P. Corvisiero, H. Constantini, A. D'Onofrio, Z. Fülöp, G. Gervino, L. Gialanella, A. Guglielmetti, C. Gustavino, G. Imbriani, M. Junker, P. G. Moroni, A. Ordine, P. Prati, V. Roca, D. Rogalla, C. Rolfs, M. Romano, F. Schümann, E. Somorjai, O. Straniero, F. Strieder, F. Terrasi, H. P. Trautvetter, and S. Zavatarelli, Nucl. Phys. A **690**, 790 (2001).

[6]H. J. Assenbaum, K. Langanke, and C. Rolfs, Z. Phys. A: Hadrons Nucl. **327**, 461 (1987).

[7]C. Broggini and LUNA Collaboration, Prog. Part. Nucl. Phys. **57**, 343 (2006).

[8]D. T. Casey, D. B. Sayre, C. Brune, V. A. Smalyuk, C. Weber, R. E. Tipton, J. E. Pino, G. P. Grim, B. A. Remington, D. Dearborn, L. R. Benedetti, J. A. Frenje, M. Gatu-Johnson, R. Hatarik, N. Izumi, J. M. McNaney, T. Ma, G. Kyrala, S. MacLaren, J. Salmonson, S. Khan, A. Pak, M. Couder, L. Berzak-Hopkins, S. LePape, B. K. Spears, N. B. Meezan, L. Divol, C. B. Yeamans, J. A. Caggiano, D. P. McNabb, D. M. Holunga, M. Chiarappa-Zucca, T. R. Kohut, and T. G. Parham, "Astrophysical S-factor Measurements at the National Ignition Facility at Density and Temperature Conditions Relevant to Stellar Cores," Nat. Phys. (submitted).

[9]M. J. Rosenberg, H. G. Rinderknecht, N. M. Hoffman, P. A. Amendt, S. Atzeni, A. B. Zylstra, C. K. Li, F. H. Séguin, H. Sio, M. Gatu-Johnson, J. A. Frenje, R. D. Petrasso, V. Yu. Glebov, C. Stoeckl, W. Seka, F. J. Marshall, J. A. Delettrez, T. C. Sangster, R. Betti, V. N. Goncharov, D. D. Meyerhofer, S. Skupsky, C. Bellei, J. Pino, S. C. Wilks, G. Kagan, K. Molvig, and A. Nikroo, Phys. Rev. Lett. **112**, 185001 (2014).

[10]V. A. Smalyuk, L. J. Atherton, L. R. Benedetti, R. Bionta, D. Bleuel, E. Bond, D. K. Bradley, J. Caggiano, D. A. Callahan, D. T. Casey, P. M. Celliers, C. J. Cerjan, D. Clark, E. L. Dewald, S. N. Dixit, T. Doüppner, D. H. Edgell, M. J. Edwards, J. Frenje, M. Gatu-Johnson, V. Y. Glebov, S. Glenn, S. H. Glenzer, G. Grim, S. W. Haan, B. A. Hammel, E. P. Hartouni, R. Hatarik, S. Hatchett, D. G. Hicks, W. W. Hsing, N. Izumi, O. S. Jones, M. H. Key, S. F. Khan, J. D. Kilkenny, J. L. Kline, J. Knauer, G. A. Kyrala, O. L. Landen, S. Le Pape, J. D. Lindl, T. Ma, B. J. MacGowan, A. J. Mackinnon, A. G. MacPhee, J. McNaney, N. B. Meezan, J. D. Moody, A. Moore, M. Moran, E. I. Moses, A. Pak, T. Parham, H.-S. Park, P. K. Patel, R. Petrasso, J. E. Ralph, S. P. Regan, B. A. Remington, H. F. Robey, J. S. Ross, B. K. Spears, P. T. Springer, L. J. Suter, R. Tommasini, R. P. Town, S. V. Weber, and K. Widmann, Phys. Rev. Lett. **111**, 215001 (2013).

[11]A. B. Zylstra, H. W. Herrmann, M. Gatu-Johnson, Y. H. Kim, J. A. Frenje, G. Hale, C. K. Li, M. Rubery, M. Paris, A. Bacher, C. Brune, C. Forrest, V. Glebov, R. Janezic, D. McNabb, A. Nikroo, J. Pino, T. C. Sangster, F. H. Séguin, W. Seka, H. Sio, C. Stoeckl, and R. D. Petrasso, Phys. Rev. Lett. **117**, 035002 (2016).

[12]A. B. Zylstra, "Using fusion-product spectroscopy to study inertial fusion implosions, stopping power, and astrophysical nucleosynthesis at OMEGA and the NIF," Ph.D. thesis, MIT (2015).

[13]M. Barbui, W. Bang, A. Bonasera, K. Hagel, K. Schmidt, J. B. Natowitz, R. Burch, G. Giuliani, M. Barbarino, H. Zheng, G. Dyer, H. J. Quevedo, E. Gaul, A. C. Bernstein, M. Donovan, S. Kimura, M. Mazzocco, F. Consoli, R. De Angelis, P. Andreoli, and T. Ditmire, Phys. Rev. Lett. **111**, 082502 (2013).

[14]J. A. Frenje, C. K. Li, F. H. Séguin, D. T. Casey, R. D. Petrasso, D. P. McNabb, P. Navratil, S. Quaglioni, T. C. Sangster, V. Yu. Glebov, and D. D. Meyerhofer, Phys. Rev. Lett. **107**, 122502 (2011).

[15]D. T. Casey, J. A. Frenje, M. Gatu-Johnson, M. J.-E. Manuel, N. Sinenian, A. B. Zylstra, F. H. Séguin, C. K. Li, R. D. Petrasso, V. Yu. Glebov, P. B. Radha, D. D. Meyerhofer, T. C. Sangster, D. P. McNabb, P. A. Amendt, R. N. Boyd, S. P. Hatchett, S. Quaglioni, J. R. Rygg, I. J. Thompson, A. D. Bacher, H. W. Herrmann, and Y. H. Kim, Phys. Rev. Lett. **109**, 025003 (2012).

[16]D. B. Sayre, C. R. Brune, J. A. Caggiano, V. Y. Glebov, R. Hatarik, A. D. Bacher, D. L. Bleuel, D. T. Casey, C. J. Cerjan, M. J. Eckart, R. J. Fortner, J. A. Frenje, S. Friedrich, M. Gatu-Johnson, G. P. Grim, C. Hagmann, J. P. Knauer, J. L. Kline, D. P. McNabb, J. M. McNaney, J. M. Mintz, M. J. Moran, A. Nikroo, T. Phillips, J. E. Pino, B. A. Remington, D. P. Rowley, D. H. Schneider, V. A. Smalyuk, W. Stoeffl, R. E. Tipton, S. V. Weber, and C. B. Yeamans, Phys. Rev. Lett. **111**, 052501 (2013).

[17]C. Angulo, M. Arnould, M. Rayet, P. Descouvemont, D. Baye, C. Leclercq-Willain, A. Coc, S. Barhoumi, P. Aguer, C. Rolfs, R. Kunz, J. W. Hammer, A. Mayer, T. Paradellis, S. Kossionides, C. Chronidou, K. Spyrou, S. Degl'Innocenti, G. Fiorentini, B. Ricci, S. Zavatarelli, C. Providencia, H. Wolters, J. Soares, C. Grama, J. Rahighi, A. Shotter, and M. L. Rachti, Nucl. Phys. A **656**, 3–183 (1999).

[18]D. G. Hicks, C. K. Li, F. H. Séguin, A. K. Ram, J. A. Frenje, R. D. Petrasso, J. M. Soures, V. Yu. Glebov, D. D. Meyerhofer, S. Roberts, C. Sorce, C. Stöckl, T. C. Sangster, and T. W. Phillips, Phys. Plasmas **7**, 5106 (2000).

[19]N. Sinenian, M. J.-E. Manuel, J. A. Frenje, F. H. Séguin, C. K. Li, and R. D. Petrasso, Plasma Phys. Controlled Fusion **55**, 045001 (2013).

[20]W. Seka, D. H. Edgell, J. F. Myatt, A. V. Maximov, R. W. Short, V. N. Goncharov, and H. A. Baldis, Phys. Plasmas **16**, 052701 (2009).

[21]R. M. Darlington, T. L. McAbee, and G. Rodrigue, Comput. Phys. Commun. **135**(1), 58 (2001).

[22]C. Forrest, R. Bahukutumbi, V. Glebov, V. Goncharov, J. Knauer, A. Pruyne, M. Romanofsky, T. Sangster, M. Shoup III, C. Stoeckl, D. Casey, M. Gatu-Johnson, and S. Gardner, Rev. Sci. Instrum. **83**, 10D919 (2012).

[23]V. Yu. Glebov, C. Stoeckl, T. C. Sangster, S. Roberts, G. J. Schmid, R. A. Lerche, and M. J. Moran, Rev. Sci. Instrum. **75**, 3559 (2004).

[24]C. Stoeckl, R. Boni, F. Ehrne, C. J. Forrest, V. Yu. Glebov, J. Katz, D. J. Lonobile, J. Magoon, S. P. Regan, M. J. Shoup III, A. Sorce, C. Sorce, T. C. Sangster, and D. Weiner, Rev. Sci. Instrum. **87**, 053501 (2016).

[25]W. Seka, H. A. Baldis, J. Fuchs, S. P. Regan, D. D. Meyerhofer, C. Stoeckl, B. Yaakobi, R. S. Craxton, and R. W. Short, Phys. Rev. Lett. **89**, 175002 (2002).

[26]A. M. Cok, R. S. Craxton, and P. W. McKenty, Phys. Plasmas **15**, 082705 (2008).

[27]D. G. Hicks, "Charged-particle spectroscopy: A new window on inertial confinement fusion," Ph.D. thesis, Massachusetts Institute of Technology (1999).

[28]L. Ballabio, J. Källne, and G. Gorini, Nucl. Fusion **38**, 1723 (1998).

[29]J. A. Frenje, P. E. Grabowski, C. K. Li, F. H. Séguin, A. B. Zylstra, M. Gatu-Johnson, R. D. Petrasso, V. Yu. Glebov, and T. C. Sangster, Phys. Rev. Lett. **115**, 205001 (2015).

[30]C. J. Waugh, M. J. Rosenberg, A. B. Zylstra, J. A. Frenje, F. H. Séguin, R. D. Petrasso, V. Yu. Glebov, T. C. Sangster, and C. Stoeckl, Rev. Sci. Instrum. **86**, 053506 (2015).

[31]J. A. Frenje, D. T. Casey, C. K. Li, J. R. Rygg, F. H. Séguin, R. D. Petrasso, V. Yu. Glebov, D. D. Meyerhofer, T. C. Sangster, S. Hatchett, S. Haan, C. Cerjan, O. Landen, M. Moran, P. Song, D. C. Wilson, and R. J. Leeper, Rev. Sci. Instrum. **79**, 10E502 (2008).

[32]F. H. Seǵuin, J. A. Frenje, C. K. Li, D. G. Hicks, S. Kurebayashi, J. R. Rygg, B.-E. Schwartz, R. D. Petrasso, S. Roberts, J. M. Soures, D. D. Meyerhofer, T. C. Sangster, J. P. Knauer, C. Sorce, V. Yu. Glebov, C. Stoeckl, T. W. Phillips, R. J. Leeper, K. Fletcher, and S. Padalino, Rev. Sci. Instrum. **74**, 975 (2003).

[33]The uncertainty is calculated as the error on the weighted mean (∼2.9%) times reduced χ^2 for the assumption that all measurements are samples of the same mean ($\chi^2_{\mathrm{red}} \sim 1.1$).

[34]M. Gatu-Johnson, C. Forrest, D. B. Sayre, A. Bacher, J.-L. Bourgade, J. A. Caggiano, D. T. Casey, J. A. Frenje, V. Yu. Glebov, R. Hatarik, H. W. Herrmann, R. Janezic, Y. H. Kim, J. P. Knauer, O. Landoas, D. P.

McNabb, R. D. Petrasso, J. E. Pino, J. Sanchez, T. C. Sangster, H. Sio, W. Shmayda, C. Stoeckl, and A. B. Zylstra, "Evidence for energy dependence in T(t,2n)α reaction channel strength at center-of-mass energies in the range 16-50 keV," Phys. Rev. Lett. (submitted).
[35]V. N. Goncharov, T. C. Sangster, T. R. Boehly, S. X. Hu, I. V. Igumenshchev, F. J. Marshall, R. L. McCrory, D. D. Meyerhofer, P. B. Radha, W. Seka, S. Skupsky, C. Stoeckl, D. T. Casey, J. A. Frenje, and R. D. Petrasso, Phys. Rev. Lett. **104**, 165001 (2010).
[36]S. LePape, A. Mackinnon, P. Mckenty, S. Craxton, S. Janezic, T. Ma, R. Tommasini, P. Patel, N. Izumi, A. Nikroo, M. Hoppe, J. Caggianno, V. Glebov, J. Frenje, H. Herrmann, J. McNanney, G. Grimm, R. Leeper, D. Bleuel, S. Friedriech, J. Knauer, R. Petrasso, H. Rinderknecht, C. Sangster, and J. D. Kilkenny, Bull. Am. Phys. Soc. **56**(16), 192 (2011); http://meetings.aps.org/link/BAPS.2011.DPP.NO6.1.
[37]P. W. McKenty, R. S. Craxton, D. H. Froula, D. T. Michel, J. A. Marozas, T. C. Sangster, D. D. Meyerhofer, R. L. McCrory, J. D. Kilkenny, A. Nikroo, M. L. Hoppe, S. LePape, A. J. Mackinnon, and D. H. Munro, Am. Phys. Soc. **57**(12), 155 (2011); http://meetings.aps.org/link/BAPS.2012.DPP.JO4.11.
[38]M. J. Rosenberg, A. B. Zylstra, F. H. Séguin, H. G. Rinderknecht, J. A. Frenje, M. Gatu-Johnson, H. Sio, C. J. Waugh, N. Sinenian, C. K. Li, R. D. Petrasso, P. W. McKenty, M. Hohenberger, P. B. Radha, J. A. Delettrez, V. Yu. Glebov, R. Betti, V. N. Goncharov, J. P. Knauer, T. C. Sangster, S. LePape, A. J. Mackinnon, J. Pino, J. M. McNaney, J. R. Rygg, P. A. Amendt, C. Bellei, L. R. Benedetti, L. Berzak-Hopkins, R. M. Bionta, D. T. Casey, L. Divol, M. J. Edwards, S. Glenn, S. H. Glenzer, D. G. Hicks, J. R. Kimbrough, O. L. Landen, J. D. Lindl, T. Ma, A. MacPhee, N. B. Meezan, J. D. Moody, M. J. Moran, H.-S. Park, B. A. Remington, H. Robey, M. D. Rosen, S. C. Wilks, R. A. Zacharias, H. W. Herrmann, N. M. Hoffman, G. A. Kyrala, R. J. Leeper, R. E. Olson, J. D. Kilkenny, and A. Nikroo, Phys. Plasmas **21**, 122712 (2014).
[39]A "proton-backlighter" platform (Ref. 40) using thin-glass-shell capsules is also being developed for NIF. In this case, the goal is to generate a small source using a minimal number of laser beams, hence, smaller targets are used (OD ∼ 400–800 μm) and the optimization goals are different, but experiences from this work can be utilized also in developing the platform for nuclear experiments.
[40]J. R. Rygg, A. B. Zylstra, F. H. Séguin, S. LePape, B. Bachmann, R. S. Craxton, E. M. Garcia, Y. Z. Kong, M. Gatu-Johnson, S. F. Khan, B. J. Lahmann, P. W. McKenty, R. D. Petrasso, H. G. Rinderknecht, M. J. Rosenberg, D. B. Sayre, and H. W. Sio, Rev. Sci. Instrum. **86**, 116104 (2015).
[41]S. Skupsky, J. A. Marozas, R. S. Craxton, R. Betti, T. J. B. Collins, J. A. Delettrez, V. N. Goncharov, P. W. McKenty, P. B. Radha, T. R. Boehly, J. P. Knauer, F. J. Marshall, D. R. Harding, J. D. Kilkenny, D. D. Meyerhofer, T. C. Sangster, and R. L. McCrory, Phys. Plasmas **11**, 2763 (2004).
[42]R. S. Craxton and R. L. McCrory, J. Appl. Phys. **56**, 108 (1984).
[43]M. Hohenberger, P. B. Radha, J. F. Myatt, S. LePape, J. A. Marozas, F. J. Marshall, D. T. Michel, S. P. Regan, W. Seka, A. Shvydky, T. C. Sangster, J. W. Bates, R. Betti, T. R. Boehly, M. J. Bonino, D. T. Casey, T. J. B. Collins, R. S. Craxton, J. A. Delettrez, D. H. Edgell, R. Epstein, G. Fiksel, P. Fitzsimmons, J. A. Frenje, D. H. Froula, V. N. Goncharov, D. R. Harding, D. H. Kalantar, M. Karasik, T. J. Kessler, J. D. Kilkenny, J. P. Knauer, C. Kurz, M. Lafon, K. N. LaFortune, B. J. MacGowan, A. J. Mackinnon, A. G. MacPhee, R. L. McCrory, P. W. McKenty, J. F. Meeker, D. D. Meyerhofer, S. R. Nagel, A. Nikroo, S. Obenschain, R. D. Petrasso, J. E. Ralph, H. G. Rinderknecht, M. J. Rosenberg, A. J. Schmitt, R. J. Wallace, J. Weaver, C. Widmayer, S. Skupsky, A. A. Solodov, C. Stoeckl, B. Yaakobi, and J. D. Zuegel, Phys. Plasmas **22**, 056308 (2015).
[44]P. B. Radha, M. Hohenberger, D. H. Edgell, J. A. Marozas, F. J. Marshall, D. T. Michel, M. J. Rosenberg, W. Seka, A. Shvydky, T. R. Boehly, T. J. B. Collins, E. M. Campbell, R. S. Craxton, J. A. Delettrez, S. N. Dixit, J. A. Frenje, D. H. Froula, V. N. Goncharov, S. X. Hu, J. P. Knauer, R. L. McCrory, P. W. McKenty, D. D. Meyerhofer, J. Moody, J. F. Myatt, R. D. Petrasso, S. P. Regan, T. C. Sangster, H. Sio, S. Skupsky, and A. Zylstra, Phys. Plasmas **23**, 056305 (2016).
[45]C. R. Brune, J. A. Caggiano, D. B. Sayre, A. D. Bacher, G. M. Hale, and M. W. Paris, Phys. Rev. C **92**, 014003 (2015).
[46]P. Descouvemont and D. Baye, Rep. Prog. Phys. **73**, 036301 (2010).
[47]S. Quaglioni and P. Navratil, Phys. Rev. C **79**, 044606 (2009).
[48]S. Quaglioni and P. Navratil, Phys. Rev. Lett. **101**, 092501 (2008).
[49]H. G. Rinderknecht, H. Sio, J. A. Frenje, J. Magoon, A. Agliata, M. Shoup, S. Ayers, C. G. Bailey, M. Gatu-Johnson, A. B. Zylstra, N. Sinenian, M. J. Rosenberg, C. K. Li, F. H. Sèguin, R. D. Petrasso, J. R. Rygg, J. R. Kimbrough, A. Mackinnon, P. Bell, R. Bionta, T. Clancy, R. Zacharias, A. House, T. Döppner, H. S. Park, S. LePape, O. Landen, N. Meezan, H. Robey, V. U. Glebov, M. Hohenberger, C. Stoeckl, T. C. Sangster, C. Li, J. Parat, R. Olson, J. Kline, and J. Kilkenny, Rev. Sci. Instrum. **85**, 11D901 (2014).
[50]T. J. Clancy, J. Caggiano, J. McNaney, M. Eckart, M. Moran, V. Y. Glebov, J. Knauer, R. Hatarik, S. Friedrich, R. Zacharias, A. Carpenter, M. J. Shoup III, T. Buczek, M. Yeoman, Z. Zeid, N. Zaitseva, B. Talison, J. Worden, B. Rice, T. Duffy, A. Pruyne, and K. Marshall, Proc. SPIE **9211**, 92110A (2014).
[51]R. Hatarik, D. B. Sayre, J. A. Caggiano, T. Phillips, M. J. Eckart, E. J. Bond, C. Cerjan, G. P. Grim, E. P. Hartouni, J. P. Knauer, J. M. Mcnaney, and D. H. Munro, J. Appl. Phys. **118**, 184502 (2015).
[52]D. T. Casey, J. A. Frenje, M. Gatu-Johnson, F. H. Séguin, C. K. Li, R. D. Petrasso, V. Yu. Glebov, J. Katz, J. Magoon, D. D. Meyerhofer, T. C. Sangster, M. Shoup, J. Ulreich, R. C. Ashabranner, R. M. Bionta, A. C. Carpenter, B. Felker, H. Y. Khater, S. LePape, A. MacKinnon, M. A. McKernan, M. Moran, J. R. Rygg, M. F. Yeoman, R. Zacharias, R. J. Leeper, K. Fletcher, M. Farrell, D. Jasion, J. Kilkenny, and R. Paguio, Rev. Sci. Instrum. **84**, 043506 (2013).
[53]M. J. Rosenberg, A. B. Zylstra, J. A. Frenje, H. G. Rinderknecht, M. Gatu-Johnson, C. J. Waugh, F. H. Séguin, H. Sio, N. Sinenian, C. K. Li, R. D. Petrasso, V. Yu. Glebov, M. Hohenberger, C. Stoeckl, T. C. Sangster, C. B. Yeamans, S. LePape, A. J. Mackinnon, R. M. Bionta, B. Talison, D. T. Casey, O. L. Landen, M. J. Moran, R. A. Zacharias, J. D. Kilkenny, and A. Nikroo, Rev. Sci. Instrum. **85**, 103504 (2014).
[54]A. B. Zylstra, J. A. Frenje, F. H. Séguin, M. J. Rosenberg, H. G. Rinderknecht, M. Gatu-Johnson, D. T. Casey, N. Sinenian, M. J.-E. Manuel, C. J. Waugh, H. W. Sio, C. K. Li, R. D. Petrasso, S. Friedrich, K. Knittel, R. Bionta, M. McKernan, D. Callahan, G. W. Collins, E. Dewald, T. Döppner, M. J. Edwards, S. Glenzer, D. G. Hicks, O. L. Landen, R. London, A. Mackinnon, N. Meezan, R. R. Prasad, J. Ralph, M. Richardson, J. R. Rygg, S. Sepke, S. Weber, R. Zacharias, E. Moses, J. Kilkenny, A. Nikroo, T. C. Sangster, V. Glebov, C. Stoeckl, R. Olson, R. J. Leeper, J. Kline, G. Kyrala, and D. Wilson, Rev. Sci. Instrum. **83**, 10D901 (2012).
[55]L. Welser-Sherrill, J. H. Cooley, D. A. Haynes, D. C. Wilson, M. E. Sherrill, R. C. Mancini, and R. Tommassini, Phys. Plasmas **15**, 072702 (2008).
[56]J. Delettrez, R. Epstein, M. C. Richardson, P. A. Jaanimagi, and B. L. Henke, Phys. Rev. A **36**, 3926 (1987).
[57]T. J. Murphy, Phys. Plasmas **21**, 072701 (2014).
[58]B. Appelbe and J. Chittenden, Plasma Phys. Controlled Fusion **53**, 045002 (2011).
[59]M. Gatu-Johnson, J. P. Knauer, C. J. Cerjan, M. J. Eckart, G. P. Grim, E. P. Hartouni, R. Hatarik, J. D. Kilkenny, D. H. Munro, D. B. Sayre, B. K. Spears, R. M. Bionta, E. J. Bond, J. A. Caggiano, D. Callahan, D. T. Casey, T. Döppner, J. A. Frenje, V. Yu. Glebov, O. Hurricane, A. Kritcher, S. LePape, T. Ma, A. Mackinnon, N. Meezan, P. Patel, R. D. Petrasso, J. E. Ralph, P. T. Springer, and C. B. Yeamans, Phys. Rev. E **94**, 021202(R) (2016).
[60]D. T. Michel, C. Sorce, R. Epstein, N. Whiting, I. V. Igumenshchev, R. Jungquist, and D. H. Froula, Rev. Sci. Instrum. **83**, 10E530 (2012).
[61]The uncertainty is calculated as the error on the weighted mean (∼7.2%) times reduced χ^2 for the assumption that all measurements are samples of the same mean ($\chi^2_{\mathrm{red}} \sim 1.2$).
[62]K. Molvig, N. M. Hoffman, B. J. Albright, E. M. Nelson, and R. B. Webster, Phys. Rev. Lett. **109**, 095001 (2012).
[63]B. J. Albright, K. Molvig, C.-K. Huang, A. N. Simakov, E. S. Dodd, N. M. Hoffman, G. Kagan, and P. F. Schmit, Phys. Plasmas **20**, 122705 (2013).
[64]J. T. Larsen and S. M. Lane, J. Quant. Spectrosc. Radiat. Transfer **51**, 179 (1994).
[65]B. Appelbe and J. Chittenden, High Energy Density Phys. **19**, 29 (2016).
[66]M. Gatu-Johnson, D. T. Casey, J. A. Frenje, C.-K. Li, F. H. Séguin, R. D. Petrasso, R. Ashabranner, R. Bionta, S. LePape, M. McKernan, A. Mackinnon, J. D. Kilkenny, J. Knauer, and T. C. Sangster, Phys. Plasmas **20**, 042707 (2013).
[67]M. M. Marinak, G. D. Kerbel, N. A. Gentile, O. Jones, D. Munro, S. Pollaine, T. R. Dittrich, and S. W. Haan, Phys. Plasmas **8**, 2275 (2001).
[68]P. B. Radha, V. N. Goncharov, T. J. B. Collins, J. A. Delettrez, Y. Elbaz, V. Y. Glebov, R. L. Keck, D. E. Keller, J. P. Knauer, J. A. Marozas, F. J. Marshall, P. W. McKenty, D. D. Meyerhofer, S. P. Regan, T. C. Sangster, D. Shvarts, S. Skupsky, Y. Srebro, R. P. J. Town, and C. Stoeckl, Phys. Plasmas **12**, 032702 (2005).
[69]P. A. Amendt, O. L. Landen, H. F. Robey, C. K. Li, and R. D. Petrasso, Phys. Rev. Lett. **105**, 115005 (2010).

[70]G. Kagan and X. Z. Tang, Phys. Lett. A **378**, 1531 (2014).
[71]H. G. Rinderknecht, M. J. Rosenberg, C. K. Li, N. M. Hoffman, G. Kagan, A. B. Zylstra, H. Sio, J. A. Frenje, M. Gatu-Johnson, F. H. Séguin, R. D. Petrasso, P. Amendt, C. Bellei, S. Wilks, J. Delettrez, V. Yu. Glebov, C. Stoeckl, T. C. Sangster, D. D. Meyerhofer, and A. Nikroo, Phys. Rev. Lett. **114**, 025001 (2015).
[72]Y. H. Kim, H. W. Herrmann, M. J. Schmitt, G. Kagan, A. M. McEvoy, N. M. Hoffman, S. Gales, A. Leatherland, M. Gatu-Johnson, J. Frenje, V. Yu. Glebov, and C. Forrest, Bull. Am. Phys. Soc. **60**, 165 (2015); http://meetings.aps.org/link/BAPS.2015.DPP.JO4.11.
[73]S. F. Khan, P. M. Bell, D. K. Bradley, S. R. Burns, J. R. Celeste, L. S. Dauffy, M. J. Eckart, M. A. Gerhard, C. Hagmann, D. I. Headley, J. P. Holder, N. Izumi, M. C. Jones, J. W. Kellogg, H. Y. Khater, J. G. Kimbrough, A. G. MacPhee, Y. P. Opachich, N. E. Palmer, R. B. Petre, J. L. Porter, R. T. Shelton, T. L. Thomas, and J. B. Worden, Proc. SPIE **8505**, 850505 (2012).